MECOSED:

MODEL FOR ESTUARINE AND

COASTAL SEDIMENT TRANSPORT

Margvelashvili N.

Version 1.0

CSIRO Marine Research
GPO Box 1538, Hobart 7001
31.03.2003
Last updated: January 2009.

This report summarises theoretical and computational aspects of the sediment transport formulation incorporated in MECOSED code. The report is organised as follows. Chapter 1 gives brief overview of the sediment transport model. Chapter 2 presents governing equations for the suspended and bottom sediment transport plus equations for the dissolved and sediment attached tracers. Key sediment processes are listed in Chapter 3. Erosion/deposition, flocculation, and settling of sediment are described in Chapters 4 and 5. The bottom boundary layer formulation is given in Chapter 6. Chapter 7 describes sorption/desorption and decay algorithms. Numerical aspects of the model implementation are given in Chapter 8.

1 MODEL OVERVIEW

MECOSED is a 1-d vertical model of coastal and estuarine sediment transport. The model was intended as an improvement to transport simulation capabilities of a 3-d coastal hydrodynamic/ water quality model MECO, developed at CSIRO, Division of Marine Research (Walker & Sherwood, 1997). MECOSED simulates vertical transport of particulate, dissolved, and sediment-bound tracers in water column and in sediment bed. The complete model consists of several modules, including sediment transport module, modules for the dissolved and the sediment-bound tracers, and the bottom boundary layer module. Hydrodynamic model simulations are required to provide MECOSED with wave and current data.

Sediment transport

The sediment transport module solves advection-diffusion equations for the mass conservation of suspended and bottom sediments, taking into account bottom exchanges through the resuspension and deposition (fig. 1.1). Suspended particles undergo turbulent mixing and settling due to gravity force. Displacement of particles in sediment bed is driven by bioturbation and consolidation. The bioturbation is represented by local diffusion. Empirical formulations are used to parameterise velocities of consolidating sediments. Cohesive sediments are either eroded or deposited depending on bottom shear stress and critical stress. A concept of equilibrium sediment distribution is used to parameterise erosion/deposition of non-cohesive sediments.

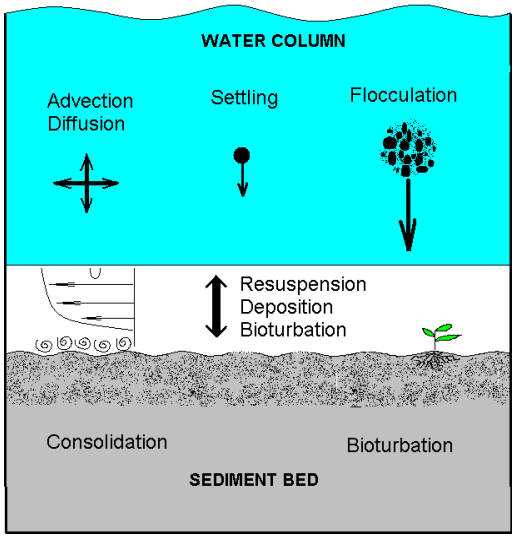

Fig. 1.1. Key sediment processes.

Dissolved transport

The module of the dissolved transport solves advection – diffusion equations of the mass conservation of tracers dissolved in water column and in sediment bed. Dissolved tracers undergo turbulent mixing in water column and bioirrigation in sediment bed. Transport in water is coupled with sediment processes through the bioirrigation and water entrainment/expulsion during resuspension/deposition or consolidation events. Bioirrigation is represented by local diffusion.

Sediment-bound tracers

The sediment-bound tracer is analogous to a hydrophobic contaminant, e.g. organic chemical, heavy metal or radionuclide that adsorb to fine-grained sediment particles. The model solves advection – diffusion equations for the mass conservation of the sediment-bound tracers in water column and in sediment bed. Sorption exchange between solid and liquid phases is simulated using the concept of the equilibrium distribution. To simulate degradable pollutants, the model incorporates first-order decay reaction.

Bottom boundary layer

Bottom friction under combined wave-current flow is estimated using Grant and Madsen (1994) model. On cohesive sediment bed constant physical roughness associated with biogenic bed-forms is specified. On non-cohesive sediment bed the total physical roughness is assumed to be composed of three components: one due to skin friction at the bed, one due to form drag over the ripples, and one due to the dissipation associated with a near bottom layer of intense sediment transport. Ripples in a wave-dominated environment are either simulated or specified as the model input data. Under combined waves and currents and in a current-dominated flow the bed forms are specified as the model input data.

Numerical solution

The model governing equations are formulated in a time-varying, sediment thickness and optionally water depth adapted coordinate frame. The numerical solution utilises implicit finite difference scheme for advective and diffusive terms. Advective terms are approximated using upwind finite difference. The governing equations are transformed to a three-diagonal system of algebraic equations, which is solved using Thompson's method.

2 TRANSPORT EQUATIONS

MECOSED solves advection-diffusion equations for multiply sediment classes (and for dissolved tracers) in both water column and sediment bed. The thickness of the sediment layer varies with time due to resuspension/deposition and consolidation of sediments. To maintain high vertical resolution near the seabed surface throughout the simulation period, the model employs stretched, depth-adjusted numerical grids. This section describes mass balance equations and boundary conditions. The next section provides grid specifications, formulations for sediment and water velocities, and resuspesion/deposition fluxes.

Here and throughout the document, solid and liquid phases are assumed to be incompressible. The vertical axis of the coordinate frame is directed upward. Sediments, dissolved tracers and tracers attached to sediments are represented by vertical profiles of the sediment concentration $C^s(z,t)$ [kg/(m^3 mixture)], the concentration of the dissolved tracer $C^d(z,t)$ [kg/(m^3 water)], and the concentration of the tracer attached to sediment $C^p(z,t)$ [kg/(m^3 mixture)]. The superscripts (s), (w), (d), and (p) denote the solid phase, liquid phase (water), dissolved phase, and tracer attached to sediment (pollutant) respectively. The subscripts (i) and (j) are introduced whenever sediments or dissolved traces are represented by a number of classes. All classes of particles in benthic layer have the same vertical velocity associated with the sediment consolidation $U_i^s \equiv U_c^s(z,t)$. The vertical velocity of all dissolved tracers equals to the water velocity $U_i^d \equiv U^w(z,t)$. Benthic and pelagic environments are represented by discrete, time-varying layers of thickness $Z_k = z_{(k+)} - z_{(k-)}$, with the subscript *k* indicating the layer number, and (k_+) and (*k*-) indexes indicating the top and the bottom interfaces between layers, respectively (Figure 1).

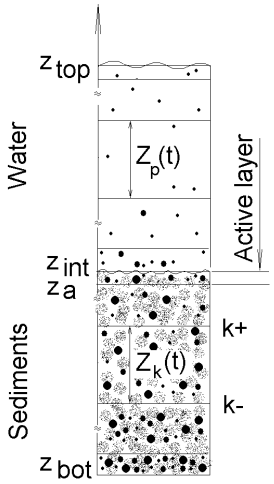

Figure 1. Coupled benthic-pelagic system sketch.

2.1 Mass conservation

A general mass balance equation for sediments ($C = C^s$), dissolved tracer ($C = C^d$), and for tracer on sediments ($C = C^p$) in a stretched Eulerian frame z=z(t), can be expressed as follows (Appendix A)

$$\frac{\partial}{\partial t}(C\cdot\varphi)=-\frac{\partial}{\partial z}\left[\varphi\left(\tilde{U}-\nu\frac{\partial}{\partial z}\right)C\right]-\varphi C\frac{\partial V_g}{\partial z} \qquad (2.1)$$

Here V_g is the velocity of the time-varying coordinate levels; $\tilde{U}=(U-V_g)$ is the velocity of either a particulate or dissolved tracer expressed in a time-varying frame $z=z(t)$; U is the tracer velocity in an immobilised frame**;** ν is the diffusion coefficient, representing either turbulent mixing in the water column or biodiffusion in the sediments. φ is the porosity when equation (2.1) is applied to the dissolved tracer, and $\varphi\equiv 1$ in the case of sediments or sediment attached tracers.

To solve equation (2.1) in both the water column ($z_{\text{int}}<z<z_{top}$) and sediments ($z_{bot}<z<z_{\text{int}}$), the location of the sediment-water interface (z_{int}) must be known. Assuming no fluxes through the lateral boundaries, and immobilised, impermeable base underlying deep sediments, the displacement of the sediment-water interface can be related to the material fluxes across the interface:

$$\frac{\partial z_{\text{int}}}{\partial t}=-(F^s+F^w). \qquad (2.2)$$

Here F^s, F^w are the area-normalised volumetric fluxes of solid and liquid phases across the water-sediment interface, respectively.

The volumetric flux of solids can be expressed as

$$F^s=\frac{Q^s}{\rho^s}, \qquad (2.3)$$

where Q^s [kg/(m^2 s)] is the resuspension or deposition flux of the sediments, and ρ^s is the density of the sediment grains.

To estimate liquid fluxes, we assume that an amount of pore water expelled from sediments during resuspension is a function of the observed sediment porosity, and an amount of water trapped in sediments during deposition is a function of the porosity of fresh sediment deposits. The corresponding fluxes can be expressed as $\left(\varepsilon Q^s/\rho^s\right)$, where ε is a void-ratio of either resuspending or settling sediments. In consolidating or swelling sediments, water exchange between benthic and pelagic layers is also influenced by an expulsion of pore-water from consolidating sediments, and entrainment of water into swelling sediments. The corresponding fluxes across the sediment-water interface can be represented as a function of the interface velocity $\left(-U_c^{\,s}\big|_{z=z\,\text{int}}\right)$, where $U_c^{\,s}$ is the velocity of consolidating or swelling particles. Combining fluxes due to resuspension/deposition and swelling/consolidation gives a net flux of water through the sediment-water interface:

$$F^w=-U_c^{\,s}\Big|_{z=z\,\text{int}}+\frac{\varepsilon Q^s}{\rho^s} \qquad (2.4)$$

2.2 Boundary conditions

There are no fluxes of any tracer through the top of the water column and through the bottom of the benthic layer:

$$\varphi\left(\tilde{U} - \nu\frac{\partial}{\partial z}\right)\cdot C = 0; \qquad z = z_{top}, \quad z = z_{bot} \tag{2.5}$$

Material fluxes across the "water-sediment" interface are specified taking into account resuspension/deposition and swelling/consolidation of sediments:

$$\varphi\left(\tilde{U} - \nu\frac{\partial}{\partial z}\right)\cdot C = \varphi\cdot q\cdot r; \qquad z = z_{\text{int}} \tag{2.6}$$

The right hand side in (2.6) represents either sediment resuspension/deposition ($q = Q^s$, $r \equiv 1$), or advection of the dissolved tracer across the sediment-water interface ($q = F^w \cdot C^d$, $r \equiv 1$), or pollutant flux $\left(q = Q^s, r = \frac{C^p}{C^s}\right)$.

Diffusion across water and sediments is incorporated into the model by adding the corresponding fluxes to q: $q = Q^s - \alpha\left(C_{wc}{}^s - C_{bed}{}^s\right)$ in the case of sediments and sediment attached tracers, and $q = F^w C^d - \beta\left(C_{wc}{}^d - C_{bed}{}^d\right)$ for the dissolved tracers. Here $C_{wc}{}^*$ and $C_{bed}{}^*$ denote concentrations in water column and sediment bed, respectively. The rate constants α and β are given by $\alpha = \nu_o{}^s\left[\min(\Delta Z_{wc}, \Delta Z_{bed})\right]^{-1}$, and $\beta = \nu_o{}^d\left[\min(\Delta Z_{wc}, \Delta Z_{bed})\right]^{-1}$, where $\nu_o{}^s$ and $\nu_o{}^d$ are vertical diffusion coefficients for solid and dissolved phases, respectively, and $\Delta Z_{wc}, \Delta Z_{bed}$ are thicknesses of the near bottom grid cells in water and in sediments, respectively.

2.3 Multi-grain-size sediments

Having sediments represented by a number of size fractions (i = 1 – n), implies that equation (2.1) with the boundary conditions (2.5, 2.6) is applied to each sediment fraction, and fluxes (2.3) and (2.4) are reformulated as follows:

$$F^s = \sum_{i=1}^{n}\frac{Q_i^s}{\rho_i^s}, \tag{2.3'}$$

$$F^w = -U_c{}^s\Big|_{z=z\,\text{int}} + \sum_{i=1}^{n}\left(\frac{\varepsilon_i Q_i^s}{\rho_i^s}\right). \tag{2.4'}$$

Here Q_i^s is the resuspension/deposition flux of the *i*-th fraction of the particulate tracer, and ρ_i^s is the density of the sediment grains, ε_i is the void-ratio of either resuspending or settling sediments.

3 Key processes and parameters

To solve (2.1-2.6), resuspension/deposition fluxes (Q^s), settling velocity of suspended sediment (U^s), velocity of consolidating particles ($U_c{}^s$), vertical water velocity (U^w), and velocity of the numerical grid levels (V_g) are required. This section outlines formulations for these variables employed in MECOSED.

3.1 Sediment velocity

There is a large body of literature concerning the settling of suspended particles in turbulent flows (e.g. Dyer, 1989; van Rijn, 1993; Thomas et al., 1999). Settling velocities are parameterised as a function of local hydrological characteristics and physical properties of the sediment grains. Different formulations are used with cohesive and non-cohesive sediments. In MECOSED a constant settling velocity is assumed for any class of non-cohesive sediments, and a number of flocculation options is available for fine cohesive particles. More detailed discussion of suspended sediment settling for cohesive and non-cohesive particles can be found below in chapters 4 and 5.

The level of accuracy and complexity in representing the velocity of bottom sediments varies from one study to another depending on data availability and modelling objectives. Geotechnical engineers have made considerable progress in understanding and predicting self-weight consolidation of fine-grained sediments (Toorman, 1996). However, modelling of natural sediments, typically represented by chemically and biologically active mixtures of water, sand, fines, and organic materials, is still in a development stage (Torfs et al., 1996; Mitchener & Torfs, 1996). In MECOSED we specify sediment velocity as a function of the sediment void ratio and assume that the void ratio in sediments gradually relaxes to a predefined ultimate value

$$\frac{\partial U_c{}^s}{\partial z} = \frac{1}{(1+\varepsilon)}\frac{\partial \varepsilon}{\partial t} \approx \frac{1}{(1+\varepsilon)}\frac{(\varepsilon-\varepsilon_m)}{T_c} \tag{3.1}$$

Here ε is the actual void ratio, ε_m is the ultimate void ratio, and T_c is the time scale of the seabed swelling or consolidation. Note that settling velocities of consolidating particles in (3.1) are the same for all sediment classes. Some justification for this choice provide laboratory studies showing that in bottom sediments represented by concentrated mixtures of particles, the sediment grains tend to form a matrix structure, which is generally able to support particles without falling through (Torfs et al., 1996).

Equation (3.1) represents mass conservation of a uniform medium with a time-varying porosity (Appendix A). To solve (3.1), the sediment velocity must be specified at the bottom of the sediment layer: $U_c{}^s = 0;\ z = z_{bot}$.

3.2 Water velocity

An equation for vertical component of the water velocity in water column and in sediments follows from the mass balance equation for the liquid phase (Appendix A):

$$-\frac{\partial\left(\varphi\tilde{U}^w\right)}{\partial z} = \frac{\partial\varphi}{\partial t} + \varphi\frac{\partial V_g}{\partial z} \tag{3.2}$$

Equation (3.2) expresses water flow as a function of the time-varying porosity and sediment thickness, and thus gives an integral representation of various specific liquid fluxes, associated with sediment erosion/deposition, swelling/consolidation, settling and bioturbation processes. To solve (3.2), the water velocity must be specified at the bottom of the sediment layer: $\varphi\tilde{U}^{w} = 0\,; z = z_{bot}$

3.3 Velocity of grid levels

To maintain high vertical resolution near the sea bed surface, MECOSED employs stretched numerical grids. In a dynamic coastal environment with frequent resuspension and deposition of sediments, such grids tend to generate large apparent fluxes between the grid layers translating into large numerical diffusion of simulated tracers. To mitigate this effect, following Margvelashvili (2008), MECOSED employs combined sigma and k-sigma grids which allow for high vertical resolution and low numerical diffusion to be maintained throughout the simulation course. More detailed description of the grid formulation is given below in chapter 7.

Having specified the grid dynamics, the velocity of grid levels is calculated as $V_g = {\partial z_{k-}}/{\partial t}$.

3.4 Resuspension and deposition fluxes

Commonly used semi-empirical formulas have been employed to represent sediment resuspension and deposition on a cohesive or non-cohesive sediment bed. On a sandy sea-bed, it is assumed that under steady, uniform flow and sediment loading conditions, an equilibrium distribution of sediments in the water column tends to be established, with the resuspension and deposition fluxes cancelling each other. An appropriate sediment flux boundary condition can be specified using the Smith and McLean formulation (Smith & McLean, 1977). In cohesive sediments the bottom boundary condition is formulated using Ariathurai & Krone (1976), and Partheniades (1965) formulations. The sediment fluxes are functions of the bottom shear stresses, which are calculated using the Grant & Madsen approach (Madsen., 1994).

More detailed description of the resuspension and deposition fluxes can be found below in chapter 4 and 5. Formulations used in bottom boundary layer module of MECOSED are presented in chapter 6.

3.5 Active layer

Processes that control the thickness of an active, top sediment layer ($h_a = z_{\text{int}} - z_a$) are not well understood. Previous methods used to prescribe the erosion depth in coastal sediments vary considerably. Reed et al. (1999) prescribed a thickness of 0.3 mm when simulating storm resuspension on the Eel River shelf (Northern California). Wiberg and Harris (2001) calculated thickness of this layer on sandy sediments as a function of mixing depth developed by migrating ripples or sheet flow. In silty sediments the active layer depth was a function of the bottom shear stress. MECOSED assumes that the thickness of the top sediment layer is constant throughout the simulation and its value must be specified through the model calibration study.

3.6 Numerical solution

During actual simulation, first the sediment concentrations in water column and in sediment bed are updated, followed by the calculation of liquid fluxes, and solution of the transport equation for the dissolved matter. The advection-diffusion equation (2.1) is expressed in a conservative form:

$$\frac{\partial}{\partial t}\left(C\cdot\varphi\cdot Z\right)_k = -\partial_z\left[\varphi\left(\tilde{U}-\nu\frac{\partial}{\partial z}\right)C\right]_k . \tag{3.3}$$

Boundary conditions for (3.3) are provided by (2.5) and (2.6). The numerical model utilises implicit finite difference schemes to approximate advective and diffusive terms. The governing equations are transformed into a system of three-diagonal, algebraic equations and solved numerically. More details on numerical implementation of MECOSED are available in chapter 7.

4 NONCOHESIVE SEDIMENT

4.1 Settling velocity

In MECOSED settling velocity of the suspended particles, rather than the particle size, is specified directly as the model input data. In many applications however data on sediment grain size are more readily available than the settling velocity. This section includes a number of formulations expressing sediment settling velocity as a function of the sediment grain size.

For a viscous Stokes regime ($\mathrm{Re} = \frac{\left|U^s\right| d}{\nu_0} < 1$) the terminal fall velocity of a sphere can be calculated as

$$\left|U^s\right| = \frac{gd^2}{18}\left(\frac{\rho^p-\rho^w}{\mu}\right) \tag{4.1}$$

where d is a diameter of the sediment particle, ν_0 is kinematic water viscosity, μ is dynamic water viscosity, and g is particles acceleration due to gravity.

Particles of different shapes have different fall velocities. For natural sand the shape effect is largest for relatively large particles (> 300 mkm) which deviate more from sphere then a small particle. Empirical formula developed by van Rijn (1993) can be used to define terminal fall velocity for natural sediment particles:

$$\left|U^s\right| = \sqrt{g'd}\begin{cases}\frac{R_d}{18}: & d \le 100\,mkm\\ \frac{10}{R_d}\left(\sqrt{1+0.01R_d{}^2}-1\right): & 100\,mkm \le d \le 1000\,mkm,\\ 1.1: & d > 1000\,mkm\end{cases} \tag{4.2}$$

where $g' = g\left(\frac{\rho^s-\rho^w}{\rho}\right)$ is the reduced gravitational acceleration and $R_d = \frac{d\sqrt{g'd}}{\nu_0}$ is a sediment grain densimetric Reynolds number.

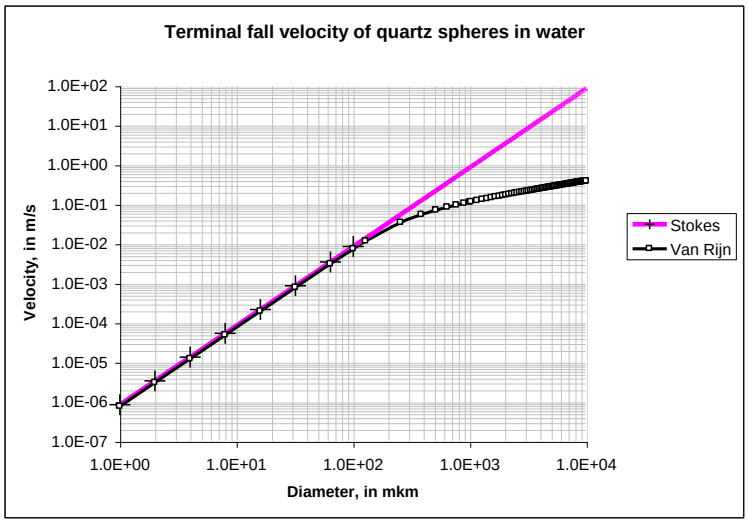

Fig. 4.1 Terminal fall velocities of quartz spheres in water calculated using Stokes and Van Rijn formulas.

The settling velocity of a single particle can be modified by the presence of other particles. This effect, known as a hindered settling, is largely caused by the fluid return flow induced by the settling particles, and can be important in the near bottom region where high concentration of sediments is common.

4.2 Critical shear stresses

Most of the sediment transport formulations are based on the Shields curve to determine the critical shear velocity for initiation of sediment motion. To avoid iterative computations required by the Shields method, Yalin's method can be used (van Rijn, 1993)

$$\begin{aligned}
\theta_{cr} &= 0.24 D_*^{-1} && 1 < D_* < 4 \\
\theta_{cr} &= 0.14 D_*^{-0.64} && 4 < D_* < 10 \\
\theta_{cr} &= 0.04 D_*^{-0.1} && 10 < D_* < 20 \\
\theta_{cr} &= 0.013 D_*^{0.29} && 20 < D_* < 150 \\
\theta_{cr} &= 0.055 && 150 < D_*
\end{aligned} \qquad (4.3)$$

where $\theta_{cr} = \dfrac{\tau_c}{(\rho^s - \rho^w) g d_{50}}$ is critical Shields parameter, $D_* = \left[\dfrac{(\rho^s - \rho^w) g}{\rho^w \nu_0^{\,2}} \right]^{1/3} d_{50}$ is particle parameter, τ_c is critical shear stress for initiation of particles motion.

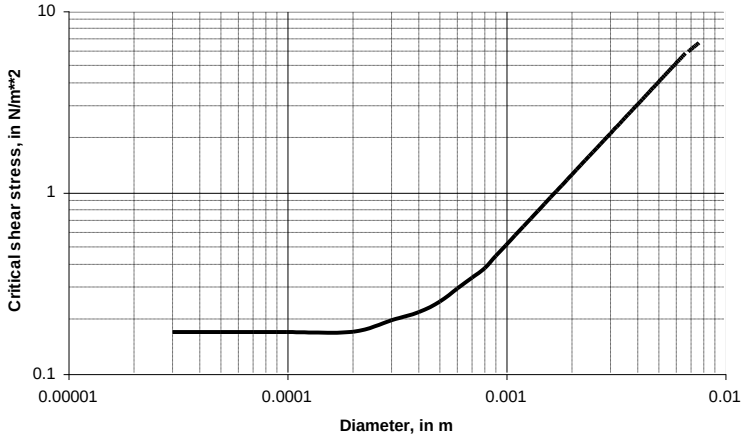

Fig. 4.2 Critical shear stress for initiation of particles motion calculated using Yalin's method.

As soon as the sediment transport process is established, ripples and dunes are formed on the bed. The critical shear stress for initiation of motion on a seabed covered by ripples is different from that for a flat bed. The bed shear stress over the rippled seabed is composed of a part related to skin friction over the bed surface and another part related to the non-uniform pressure distribution over the bed form crest and eddy regions. A sediment particle resting on the surface of a bed form will be set in motion by the skin friction force or by the turbulent fluctuations in the eddy regions downstream the crest. For increasing values of the bed shear velocity, the particles will be moving along the bed by more or less regular jumps (saltation). When the value for the bed shear stress becomes comparable with the particle fall velocity, the sediment particles may go into suspension. The criterion for initiation of suspension is

$$\left|\frac{u_{*c}}{U^s}\right| = 1 \qquad (4.4)$$

Another criteria for initiation of the suspension based on stability analysis was given by Engelund (1965) (as cited in van Rijn, 1993):

$$\left|\frac{u_{*c}}{U^s}\right| = 0.25 \qquad (4.5)$$

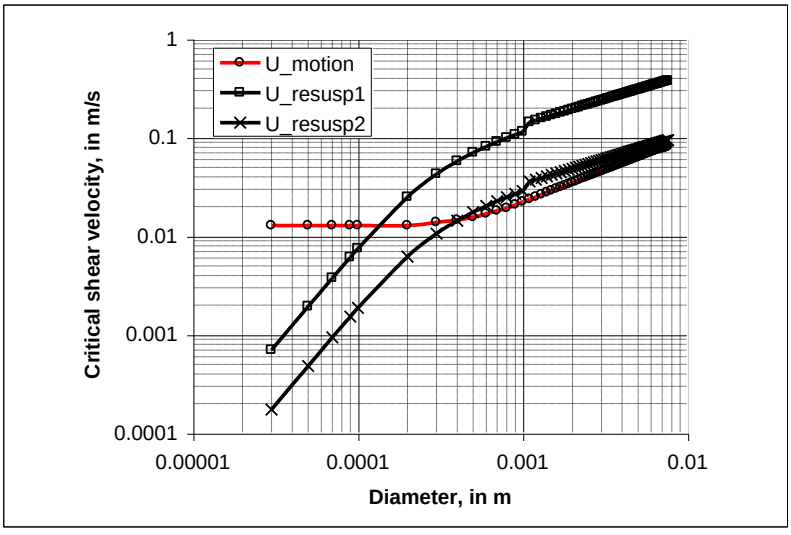

Fig. 4.3 Critical shear velocities for initiation of particles motion and sediment resuspension, calculated using formulas (4.3, 4.4, 4.5).

Fig. 4.3 shows critical shear velocities for initiation of particles motion and for sediment resuspension based on formulas (4.3-4.5). According to these formulas shear velocity required for initiation of the sediment motion can exceed the critical shear of resuspension.

4.3 Deposition and Resuspension

When the bed shear velocity exceeds the settling velocity, noncohesive sediment are resuspended and transported as suspended load. When the bed shear velocity falls below both settling velocity and the critical Sheld's shear velocity, suspended sediment deposit to the bed. A consistent formulation of these processes can be developed using the concept of a near bed equilibrium sediment concentration. Under steady, uniform flow and sediment loading conditions, an equilibrium distribution of sediments in water column tends to be established, with the resuspension and deposition fluxes cancelling each other. In terms of equilibrium sediment concentration an appropriate sediment flux boundary condition can be formulated as

$$Q_i^{\ s} = U_i^{\ s}(C_{i,r}^{\ s} - C_{i,eq}^{\ s}) \tag{4.6}$$

where $C_{i,r}^{\ s}$ is an actual concentration of sediments at the reference level z_r, and $C_{i,eq}^{\ s}$ is an equilibrium reference concentration.

An equilibrium sediment concentration can be found using (Smith J.D., McLean S.R., 1977) formula

$$C_{eq}^{\ s}(z_r) = \begin{cases} C_{bi}^{\ s}\dfrac{a \cdot S_i'}{1 + a \cdot S_i'} & S_i' > 0 \\ 0, & S_i' < 0 \end{cases} \tag{4.7}$$

where S_i' is a normalised excess skin friction, defined for each sediment class I, as

$$S_i' = \frac{|\tau_{bi}^{'}| - |\tau_{ci}|}{|\tau_{ci}|} \tag{4.8}$$

$\tau_{bi}^{'}$ is the skin friction, which is calculated through the bottom boundary layer model, τ_{ci} is critical shear stress for initiation of the sediment erosion (currently $\tau_{ci} = \rho_i\left(0.25U_i^{\ s}\right)^2$), Cbi is sediment concentration in the bed, and a is a constant of the order of 10-3. Following to (Glenn S.M., Grant W.D., 1987) an approximate value of a = 0.002 is adopted. The reference height z_r is usually specified at the distance of 7*d above the sediment bed (Coastal Engineering Manual, 1999). Another common semi-empirical method to evaluate the equilibrium concentration is based on the formulation developed by Van Rijn (1984a, 1984b). Currently MECOSED employs only Smith and McLean formulation (1977).

Sediment concentration at the reference height is estimated as (Appendix E):

$$C_r^{\,s}(z_r) = I_2\left(\frac{1}{z_r+\delta}\right)^{p+1}, \qquad I_2 = \frac{DC_0^{\,s}\,p\delta^{\,p}}{1-\left(\frac{\delta}{D+\delta}\right)^{p}}, \qquad p \neq 0 \tag{4.9}$$

$$C_r^{\,s}(z_r) = I_2\frac{1}{z_r+\delta}, \qquad I_2 = \frac{DC_0^{\,s}}{\ln\left(\frac{D+\delta}{\delta}\right)}, \qquad p = 0 \tag{4.10}$$

Here $C_0^{\,s}$ is sediment concentration averaged over the near bottom cell, $C_1^{\,s}$ is the sediment concentration at the height H, D is a height of the near bottom cell, $\nu = \kappa u_* z + \nu_0$ is turbulent diffusion coefficient, ν_0 is the diffusivity coefficient in a viscous sublayer, κ is van Karman constant, u_* is shear velocity, $\delta = \frac{\nu_0}{\kappa u_*}$ (m), $\gamma = \frac{\left|U^s\right|}{\nu_0}$ (1/m), $p = -(1-\delta\gamma)$.

5 COHESIVE SEDIMENT

Cohesive sediments do not act as separate individual particles but stick together. The degree of cohesion rises with the proportion of clay minerals in the sediment and starts becoming significant when the sediment contains more than 5 – 10 % of clay by weight (Mitchener H, Torfs H., 1996). Fresh mud deposits have a very loose texture of mud flocs and erosion can occur easily. If the deposits are not eroded again, its density gradually increases as interstitial water is pressed out of the fresh soil by the weight of the deposit itself. With the compaction of the soil the resistance to the erosion rapidly increase. In a water column cohesive sediment particles stick together forming aggregates known as flocs whose size and settling velocity are much larger than those of the individual particles.

5.1 Flocculation and Settling

The transport and fate of fine grained sediment in estuarine and coastal waters is a function of the effective settling velocity of the sediment, which in turn is affected largely by flocculation effects. The first major attempt at modelling the flocculation process was made by Smoluchowski in 1917. The equations in Smoluchowski's model have formed the core of almost all subsequent research into flocculation modelling. Brief review on flocculation modelling is available in (Thomas et al, 1999).

The mathematical representation of flocculation process conventionally is based on considering the process as two discrete steps: transport and attachment. The transport step, leading to the collision of two particles, depends on three processes: (a) the random thermal "Brownian" motion of the particles, (b) imposed velocity gradients from mixing, (c) differences in the settling velocities of individual particles (differential settling). Attachment is then parameterised by an efficiency coefficient accounting for the fact that not all encounters result in coagulation. The efficiency coefficient is a function of the physico-chemical properties of sediments and water, and of the organic compounds (coatings, polysaccharides, etc.) in the sediment. Hence it is basically an empirical parameter.

Unfortunately, the computational intensity of the approaches based on Smoluchovski's model precludes direct simulation of flocculation in operational cohesive sediment transport models for the immediate future. An alternative approach, which has met a reasonable success, is the parameterisation of the settling velocity of flocs in terms of particles primary size d, concentration C, and flow characteristics such as shear stress or

turbulence intensity in the water column or near the sediment bed. Semi-empirical expressions having the functional form

$$U^s = U^s\left(d, C^s, \frac{\partial U}{\partial z}, q\right) \tag{5.1}$$

Have been developed to represent the effective settling velocity.

The simplest and the most common way to use expression (5.1) is to replace constant settling velocities in the transport equations by effective settling velocities. Such substitution is valid when the typical time scales for the particles flocculation and break up are less than the typical time scale of the sediment advection or settling. In this case the flocs parameters can be determined from the local hydro-physical data neglecting advection and kinetics of the particles aggregation. In a deep sea environment one may speculate that most flocs are created in surface layer and then settle on the seabed without been broken up into smaller ones (Jankowski et al., 1994). Therefore floc size is not always function of local parameters and more flexible formulation of settling, taking into account advection and kinetics of the sediment flocculation and break up are required.

A number of empirical formulas, with different levels of complexity, have been developed to predict settling velocities of the sediment flocs. The most common and simple formula is based on an assumption that the flocculation and therefore also the mean settling velocity are scaled by the sediment concentration:

$$\left|U^s\right| = a\left(C^s\right)^b \tag{5.2}$$

Here a and b are empirical constants (Dyer, 1989).

Another heuristic formula was advocated by Van Leussen (cited in Winterwerp, 1998)

$$\left|U^s\right| = \left|U_0{}^s\right| \frac{1 + aG}{1 + bG^2} \tag{5.3}$$

where U^s and $U_0{}^s$ are an actual and reference settling velocities respectively, a and b are empirical parameters, and G is dissipation parameter defined as

$$G = \sqrt{\frac{e}{\nu}} = \frac{\nu}{\lambda_0{}^2} \tag{5.3'}$$

where e is the dissipation rate (m^2/s^3), ν is kinematic viscosity, and λ_0 is Kolmogorov micro-scale of turbulence. Malcherek used (5.3) with the following parameters: a = 0.3, b = 0.09, and $W_{g0} = 0.035 \cdot C$.

Empirical formula for the settling velocity of the sediment flocs based on observations in the Brisbane estuary and Moreton Bay (eastern Australia) has been developed by You et al, (1999; see also Howes, 2002):

$$\mathbf{U^s = U_0 \exp(0.945C - 0.105C^2)}. \tag{5.4}$$

Here U^s is a settling velocity of flocs, $U_0{}^s$ is a flocculation parameter representing settling velocity of individual sediment grains, and C is a concentration of suspended sediments. This flocculation formula is based on settling tests conducted on sediments from the Brisbane river and was found to fit the settling velocity of mud from Moreton Bay for concentrations of up to 9g/l.

5.2 Critical shear stresses

When the bottom consists of clay and silty materials, cohesive forces between the sediment particles become important. These forces cause a distinct increase of the resistance of the soil against erosion. Simple relationship between the critical surface erosion stress and the dry density of the bed has been proposed by Okenden and Delo (as cited in Mitchener and Torfs, 1996; and Cancino & Neves, 1999)

$$\tau_{ce} = 0.0012 \cdot \rho_d{}^{0.5} \tag{5.5}$$

where ρ_d is dry density of the sediment bed

$$\rho_d = \frac{\rho^s}{1+\varepsilon}.$$

Mitchener and Torfs (1996) advocated another experiment based formula for critical surface erosion stress in artificial sediment bed

$$\tau_{ce} = 0.015(\rho_b - 1000.)^{0.75} \tag{5.6}$$

Here ρ_b is the bulk density of the bed

$$\rho_b = \frac{\varepsilon\rho^w + \rho^s}{1+\varepsilon}.$$

Hwang and Mehta (1989) proposed the following relationship

$$\tau_{ce} = 0.883(0.001 * \rho_b - 1.065)^{0.2} + 0.05 \tag{5.7}$$

Note that dependence on the sediment density in (5.6 – 5.7) implies that this density must be known either from observations or from the model evaluations (eg through the sediment consolidation model). Critical shear stresses predicted by (5.5-5.7) are illustrated in Fig. 5.1.

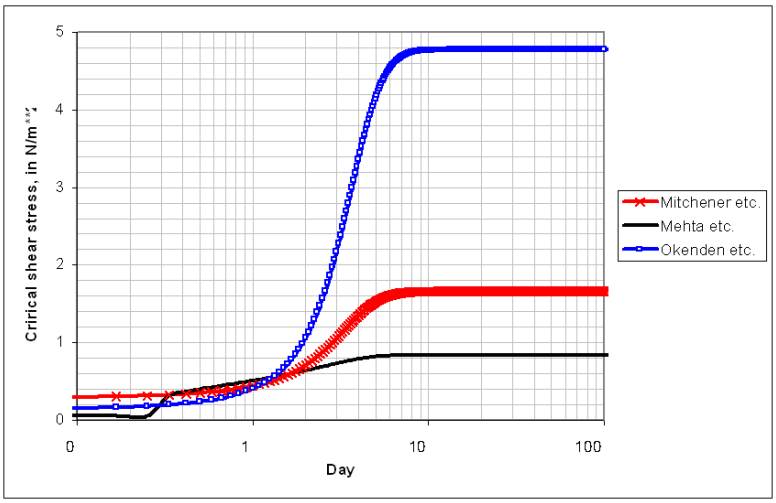

Fig. 5.1 Critical shear stress as a function of the sediment layer age.
Initial void ratio ε_0 =50, minimal void ratio ε_m =1.6. Consolidation rate constant a = 1 day

5.3 Deposition and Resuspension

Erosion and deposition of fine sediments on cohesive bed are distinctly different from those on sandy bed (Mehta et al., 1989). On cohesive beds, the erosion process might be irreversible because, once eroded, the cohesive sediment cannot be reconstituted in their consolidated form, particularly in the energetic coastal or estuarine environment. Therefore erosion is not balanced by equal volume of deposition. The eroded fine sediments (silt and clay) are winnowed, carried out and deposited in deep or still water.

Erosion and sedimentation at the sediment-water interface are functions of the bed shear stress τ_b, the critical shear stress of deposition τ_{cd}, and the critical shear stress of erosion τ_{ce}. If $\tau_b > \tau_{ce}$ erosion occurs from the top of the bed downward until the shear stress applied to bed is equal to the bed shear strength. If $\tau_b < \tau_{cd}$ the sediment will be deposited. The deposited mass of sediment forms a bed with increased values of void ratio. Due to the self-weight of the sediment mass, consolidation begins and the bed properties change. When $\tau_{cd} < \tau_b < \tau_{ce}$, the applied stress is high enough to prevent any deposition from occurring, but not high enough to erode even the top bed layer. This situation occurs when the bed has been eroded to a layer that is sufficiently hard to resist further erosion. Neither erosion nor deposition occurs during this time step, and only consolidation takes place.

The bottom boundary condition for cohesive sediments is formulated as follows (Ariathurai & Krone 1976, Partheniades 1965)

$$Q_i^s = U_i{}^s C_i{}^s f_d + \left(\frac{C^s{}_{bed,i} / \rho_i^s}{1-\varphi} \right) M f_e \qquad (5.8)$$

Where the probabilities for deposition and erosion are given by

$$f_d = \begin{cases} 0: & \tau_b \geq \tau_{cd} \\ \left(1 - \frac{\tau_b}{\tau_{cd}}\right): & \tau_b < \tau_{cd} \end{cases} \qquad f_e = \begin{cases} 0: & \tau_b < \tau_{ce} \\ \left(\frac{\tau_b}{\tau_{ce}} - 1\right): & \tau_b \geq \tau_{ce} \end{cases} \qquad (5.9)$$

The resuspension rate M (kg m^2 s^{-1}) and the critical stresses τ_{ce} and τ_{cd} must be obtained from empirical formulations. A short review of literature values of M is given in Uncles and Stephens (1989) At present the sediment model uses formulation suggested by Delo (1988) (cited in Uncles and Stephens, 1989):

$$M = 0.002 * \tau_{ce} \quad (\text{kg m}^2\ \text{s}^{-1}) \qquad (5.10)$$

The definition of the critical shear stress for erosion has been discussed above. Critical shear stress for deposition is commonly approximated by constant value. Based on laboratory experiments with natural mud from the Western Scheldt, Winterwerp et al. (1991) found τ_{cd} =0.2 N/ m^2. For Gironde Estuary Li et al. (1994) used values in the range 0.3-0.5 N/ m^2. Govindaraju et al. (1999) in modelling study for Canaveral Harbor used τ_{cd} =1.43 N/ m^2. In MECO critical shear stress of deposition is considered as a user specified, input parameter.

5.4 Mixed bed

Because of distinctly different properties of fine and coarse sediments, historically, erosion / deposition studies have concentrated largely on the behaviour of either cohesive or cohesionless sediments. However, natural sediments rarely consist of only mud or sand and in many applications erosion/deposition parameterisation for combined fine and coarse sediments is required so that the whole spectrum of natural sediment size combinations can be modelled. Unfortunately there still exists a lack of knowledge and hence theories concerning the erosion / deposition processes on a mixed sediment bed.

In MECOSED resuspension and deposition of each sediment fraction is treated individually using formulations developed for either cohesive or non-cohesive sediments. When fine particles are resuspended from the upper most active layer, coarse sediment left in this layer provide armoring of underlying sediments.

6 BOTTOM BOUNDARY LAYER

Bottom friction in a turbulent flow depends on bottom roughness. Ripples and bedload tend to dominate roughness on sandy beds, whereas bioturbated mounds typically dominate roughness of fine-sediment, cohesive beds (Li & Amos, 2001). On sandy sediments ripples start to form as the friction at the bed exceeds the threshold of sediment motion. The appearance of the ripples changes the appearance of the bottom to the flow above, as the flow resistance on the rippled bed will primarily be composed of pressure drag forces on the bed forms rather then of drag forces on individual sediment grains. Despite the increased bottom roughness associated with a rippled bed, the drag force acting on individual sediment grains and not the drag force on the bed forms is responsible for the sediment motion caused by the flow. The concept of partitioning bottom shear stress into a skin friction that moves sediment and a form drag has received considerable attention in the context of sediment transport mechanics in steady turbulent flow (Coastal Engineering Manual, 1999). Under energetic conditions the ripples wash away and the bed transport mode goes into “sheet flow” regime. The increased dissipation during “sheet flow” regime is associated with the momentum transfer by saltating particles.

Another important physical process influencing bottom roughness and friction is interaction of surface waves with low frequency currents (Grant & Madsen 1986). The wave –current interaction is associated with the nonlinear coupling of the wave and current turbulent

boundary layers. Because of the short time scale of the wave oscillations, the region in which the shear stress associated with the wave motion is significant, i.e., the wave turbulent boundary layer, is confined to a relatively thin region close to the seabed. Turbulent diffusion above the wave boundary layer, i.e., the potential flow region for the wave, is associated with the mean current only. The increased turbulent diffusion of low-momentum fluid within the wave boundary layer causes the current above the wave boundary layer to appear to feel a much greater bottom roughness than physically exists.

6.1 Ripple predictor

On many shelves and estuaries, bed ripples are dominantly wave-formed bed-forms. Ripples adjust to orbital motion in three different ranges (Li et al., 1996). In the first equilibrium range when the flow is relatively slow, both ripple height and length tend to increase with orbital excursion until ripple steepness reaches its maximum. When flow strength increase, ripples form in the second "breakoff" range where ripple height diminishes, but ripple length stay approximately constant with increasing orbital current intensity. Under high wave energy conditions the ripples wash away and the bed transport mode goes into third "planar" or "sheet flow" regime. An instability mechanism that controls the bed forms is poorly understood. Hence, empirical formulations are commonly used to evaluate ripples dimension, as well as the roughness length associated with the bed forms.

Skin friction on a rippled sediment bed depends on ripples geometry, which in turn depends on shear stresses, including skin friction. The feedback between stresses and bed forms requires iterative solution for bottom friction over the rippled sea bed. Harris and Wiberg (2001) advocate empirical predictor for ripples in a wave-dominated environment which estimates bed forms using surface wave and sediment characteristics only. An alternative formulation has been developed by Wikramanayake (1993) (as cited in Black and Oldman, 1999). Recent field measurements have shown that wave ripple predictors are not applicable to combined waves and currents. Li and Amos (2001) have developed ripple predictor for combined wave-current flow, which requires iterative assessment of various shear stresses to come up with an estimate of the ripple characteristics.

MECOSED employs the Wikramanayake (1993) ripples predictor to calculate bed forms in a wave dominated environment. Under combined wave-currents or current-dominated flows the bed forms are specified as the model input data.

Wiberg and Harris (1994, 2001).

Estimates of wave-formed, symmetric ripple height and spacing are calculated from sediment size and wave orbital velocity data. Following Wiberg and Harris (1994) the ripple spacing is expressed as

$$\lambda = 535d\,, \tag{6.1}$$

and ripple steepness as

$$\frac{\eta}{\lambda} = \exp\left[-0.095\left(\ln\frac{D}{\eta}\right)^2 + 0.442\ln\left(\frac{D}{\eta}\right) - 2.28\right], \tag{6.2}$$

where d is mean grain size and $D = (u_b T_{avb} / \pi)$ is wave orbital diameter.

Using this relationships ripple height will decrease under energetic waves with large orbital velocities.

Wikramanayake (1993)

The Wikramanayake formula includes a nondimensional parameter:

$$Z = \frac{\theta'_w 4\nu}{\sqrt{(s-1)gd^3}} \tag{6.3}$$

where θ'_w is the skin friction Shields parameter

$$\theta'_w = \frac{0.5 f_w u_b^{\ 2}}{(s-1)gd} \tag{6.4}$$

where v is the kinematic viscosity, ub is the representative bed orbital velocity, d is the median grain size, g is acceleration due to gravity, and s is the relative density of sediment. The Shields parameter includes a wave friction factor (fw) which can be specified from the empirical relationship (6.19).

The ripple height and length are defined in ranges:

$$\eta = 0.018 \frac{u_b}{\omega} Z^{-0.50}$$
$$\lambda = 0.120 \frac{u_b}{\omega} Z^{-0.49} \qquad 0.0016 < Z < 0.012 \tag{6.5}$$

$$\eta = 0.0007 \frac{u_b}{\omega} Z^{-1.23}$$
$$\lambda = 0.0677 \frac{u_b}{\omega} Z^{-0.58} \qquad 0.012 \le Z < 0.18 \tag{6.6}$$

$$\eta = 0.0$$
$$\lambda = 0.0 \qquad 0.18 \le Z \tag{6.7}$$

Beyond a value of Z=0.18, it is assumed that sheet flow conditions apply and that ripple height and length are zero.

Physical roughness

Skin roughness length is estimated from the sediment grain size as

$$k_{bs} = d$$

The physical roughness length for bedforms is estimated following Grant and Madsen (1982)

$$k_{br} = 27.7\eta\left(\frac{\eta}{\lambda}\right) \tag{6.8}$$

"Sheet flow" regime

Several studies have shown that the friction factor at hight-transport stages depends on the thickness of the bed load layer and that the transport related shear stress due to combined grain and bed load roughness should be used for predicting ripple geometry and onset of sand suspension and sheet flow transport (Li and Amos, 2001). Roughness due to saltating sediment can be estimated following Wiberg and Rubin (1989) and added to the form drag roughness. Note that ripples tend to dominate the roughness when they are present, eg in low and moderate shear stress environment, while at high shear stress the sediment transport dominates the roughness (ripples are of small steepness in this range).

6.2 Shear stresses

Bottom friction under combined waves and currents is estimated in MECOSED through the Grant and Madsen model (Madsen, 1994) which takes into account nonlinear interaction between waves and currents within the bottom boundary layer. The model is applicable only when the bottom physical roughness scale does not exceed the thickness of the wave bottom boundary layer. "This limitation is not unique to this class of models. It is inherent in all theoretical formulations of turbulent boundary layer flow that apply no-slip condition at some reference level, and may, for large roughness lead to nonsensical result of a boundary layer sickness less than the physical scale of bottom roughness elements. When the predicted thickness of the boundary layer is not large relative to the physical scale of the bottom roughness, assuming a horizontally uniform flow is a poor assumption. This issue is particularly important in the context of wave-current interaction in the coastal environment where wave-generated bedforms (ripples) create a large bottom roughness. More theoretical and experimental studies are required to shed some light on this problem…" (Madsen, 1994).

An alternative option to estimate bottom shear stress (available in MECOSED) is based on log-profile approximation of currents over the ripples and Swart's (1974) (as cited in Black and Oldman, 1999) formulation for the wave induced friction over the sediment grains. A net friction is represented as a linear combination of the current friction over the ripples and the wave friction over sediment grains. The model requires two roughness scales, one associated with individual grains and another associated with the bedforms.

Shear stresses under combined wave-current flow (Grant and Madsen model)

Following Madsen (1994), we estimate bottom shear stress under combined waves and currents as follows.

The representative shear velocity is obtained from

$$u^{2}{}_{*r} = \frac{1}{\rho}\left|\tau_{wr}\{1,0\} + \tau_{c}\{\cos\varphi_{cw}, \sin\varphi_{cw}\}\right| = C_{\mu}u^{2}{}_{*wm} \qquad (6.9)$$

in which $u_{*wm} = \sqrt{\tau_{wr}/\rho}$ is the shear velocity based on the maximum representative wave-associated shear stress (τ_{wr}),

$$C_{\mu} = \left(1 + 2\mu\left|\cos\varphi_{cw}\right| + \mu^{2}\right)^{1/2} \qquad (6.10)$$

and

$$\mu = \tau_{c}/\tau_{wr} = \left(\frac{u_{*c}}{u_{*wm}}\right)^{2} \qquad (6.11)$$

expresses the ratio of current (τ_c) and wave (τ_{wr}) bottom shear stresses; a ratio which generally is much smaller than unity and therefore results in values of C_μ, given by (6.10), close to unity. φ_{cw} gives angle between current direction and direction of wave propagation.

To obtain the maximum wave shear stress, the wave friction concept in the presence of a current is introduced through the definition

$$\frac{\tau_{wr}}{\rho} = u^2{}_{*wm} = \frac{1}{2} f_{wc} u^2{}_{br} \tag{6.12}$$

where u_{br} is the near-bottom orbital velocity amplitude. The wave friction factor as a function of relative roughness can be evaluated by the following formula

$$f_{wc} = \begin{cases} C_\mu \exp\left\{7.02\left(\dfrac{C_\mu u_{br}}{k_N \omega_r}\right)^{-0.078} - 8.82\right\}, & 0.2 < \left(\dfrac{C_\mu u_{br}}{k_N \omega_r}\right) < 10^2 \\ C_\mu \exp\left\{5.61\left(\dfrac{C_\mu u_{br}}{k_N \omega_r}\right)^{-0.109} - 7.30\right\}, & 10^2 < \left(\dfrac{C_\mu u_{br}}{k_N \omega_r}\right) < 10^4 \end{cases} \tag{6.13}$$

Here ω_r is wave radian frequency, $k_N = 30 z_o$ is equivalent Nikuradse sand grain roughness; $\chi = 0.4$ is von Karman's constant. The wave boundary layer thickness is determined from the following expression

$$\delta_{wc} = \begin{cases} \dfrac{\chi u_{*r}}{\omega_r}, & \left(\dfrac{C_\mu u_{br}}{k_N \omega_r}\right) > 8 \\ k_N, & \left(\dfrac{C_\mu u_{br}}{k_N \omega_r}\right) \le 8 \end{cases} \tag{6.14}$$

$$u_{*c} = \frac{u_{*r}}{2} \frac{\ln(z_r / \delta_{wc})}{\ln(\delta_{wc} / z_0)} \left(-1 + \sqrt{1 + \frac{4\chi \ln(\delta_{wc} / z_0)}{(\ln(z_r / \delta_{wc}))^2} \frac{u_{cr}}{u_{*r}}} \right) \tag{6.15}$$

The apparent bottom roughness experienced by currents in presence of waves is obtained by matching the current velocities at the edge of the wave boundary layer

$$\ln\left(\frac{\delta_{wc}}{z_{0A}}\right) = \frac{u_{*c}}{u_{*r}} \ln\left(\frac{\delta_{wc}}{z_0}\right) \tag{6.16}$$

The iterations are started by $\mu = \mu^{(0)} = 0$ and $C_\mu = C_\mu{}^{(0)} = 1$ from (6.10) resulting in $f_{wc} = f_{wc}{}^{(0)}$ from (6.13) and then $u_{*wm} = u_{*wm}{}^{(0)}$ from (6.12) followed by $u_{*r} = u_{*r}{}^{(0)}$ from (6.9). For the initial iteration $u_{*r} = u_{*r}{}^{(0)}$ in (6.14) and (6.15) yields the first approximation for the current shear velocity $u_{*c} = u_{*c}{}^{(0)}$. With $u_{*c} = u_{*c}{}^{(0)}$ and $u_{*wm} = u_{*wm}{}^{(0)}$ the value of

μ may be updated by use of (6.11) and the procedure may be repeated until convergence is achieved $(f_{wc}^{(n)} \approx f_{wc}^{(n+1)})$.

Wave dominated environment

Velocity and shear stress vary through the wave period, but it is common to parameterise initial motion and suspension conditions under waves in terms of the maximum boundary shear stress, or maximum shear velocity (Wiberg, Harris 1994). The magnitude of the maximum shear velocity under the wave can be expressed as

$$u_{*wm} = \sqrt{\tau_{wr} / \rho} = (f_w / 2)^{1/2} u_{br} \tag{6.17}$$

where the near-bed orbital wave velocity amplitude u_{br}, in the case of monochromatic and linear waves, can be determined from

$$u_{br} = \frac{a\omega}{2\sinh(kH)} \tag{6.18}$$

Here k is the wave number, $\omega = \frac{2\pi}{T}$ is the wave radian frequency, T is the wave period, H is the water depth, and a is the wave height.

The expression for the wave friction factor given by Grant, Madsen model (6.13) is of the same type as that proposed for a pure wave environment by Swart (1974)

$$f_w = \exp\left[5.213\left(\frac{k_b}{a_S}\right)^{0.194} - 5.977\right] \tag{6.19}$$

where the skin friction equivalent roughness $k_b = 2.5d$ is proportional to the mean grain diameter, and the half orbital excursion is given by $a_S = \frac{u_{br}}{\omega}$.

Note that the wave friction factor in a pure wave environment can also be evaluated using Grant, Madsen formulation (6.13) with $C_\mu = 1.$

Current dominated environment

For the current dominated case the log-law is used to estimate skin friction

$$u_{*c} = \chi u_r / \ln(z / z_o) \tag{6.20}$$

where $z_o = \frac{k_N}{30}$, $k_N = d$, and d is mean diameter of sediment grains.

7 REACTION TERMS

7.1 Sorption-desorption

Simulation of pollutants has become common over the last decades (Ambrose et al, 1993; Onishi et al., 1981, 1989; Shrestha & Orlob 1989; Zheleznyak et al., 1992). At minimum, the pollutant models include both chemical degradation and sorption to solids. Sorption is the bounding of dissolved chemicals onto solid phase, such as benthic or suspended sediment, colloidal organic material or biological material. It can be important in controlling both the environmental fate and toxicity of pollutants. Sorption may cause the chemical to accumulate in bed sediment or bio-concentrate in fish.

If sorption reaction is fast relative to other environmental processes an equilibrium distribution between the liquid and solid phases may be assumed (Ambrose et al., 1993). For low concentrations equilibrium sorption is linear with dissolved pollutant concentration

$$K_d = \lim_{t\to\infty}\left(\frac{\hat{C}^p}{\hat{C}^d}\right), \tag{7.1}$$

where K_d [m^3/kg] is the distribution coefficient, $\hat{C}^p$ [A/kg (dry sediment)] is pollutant concentration, A is the pollutant mass or some measure of the pollutant activity, $\hat{C}^d$ [A/m^3 (volume of water)] is the concentration of the dissolved fraction.

At equilibrium the distribution of concentrations between liquid and solid phases is controlled by the distribution coefficient K_d. However the total mass of dissolved and adsorbed pollutants, per unit volume of sediment-water mixture, is controlled by K_d and the amount of solid phase present

$$\frac{C^s}{\varphi}K_d = \lim_{t\to\infty}\left(\frac{C^p}{C^d}\right) \tag{7.2}$$

where $C^p = C^s \cdot \hat{C}^p$ [A/m^3 (volume of mixture)] is pollutant concentration, $C^d = \varphi \cdot \hat{C}^d$ [A/m^3 (volume of mixture)] is the concentration of the dissolved fraction, C^s [kg/m^3 (volume of mixture)] is sediment concentration, and por is porosity.

In addition to the assumption of instantaneous equilibrium, implicit in the use of equation (7.1) is the assumption of reversibility. Laboratory data for radionuclides and some chemicals suggest, however, that a hysteresis exist, with desorption being a much slower process than adsorption. In the simplest linear case the kinetics of sorption can be represented by first order reaction

$$\frac{\partial C^d}{\partial t} = -a\left(\frac{C^s}{\varphi}K_d C^d - C^p\right) \tag{7.3}$$

$$\frac{\partial C^p}{\partial t} = a\left(\frac{C^s}{\varphi}K_d C^d - C^p\right) \tag{7.4}$$

where a is the sorption/desorption rate constant.

$$a = \begin{cases} a_{1,2}, & \frac{C^s}{\varphi} K_d C^d > C^p \\ a_{2,1}, & \frac{C^s}{\varphi} K_d C^d <= C^p \end{cases} \qquad (7.5)$$

These governing equations are similar to those used in (Onishi et al., 1981, 1989; Shrestha & Orlob 1989; Zheleznyak et al., 1992, Margvelashvili et al., 1997).

The analytical solution of (7.3, 7.4) is:

$$C^d = A_o \exp\left[-a\left(\frac{C^s}{\varphi} K_d + 1 \right) t \right] + B_o \qquad (7.6)$$

$$C^p = -A_o \exp\left[-a\left(\frac{C^s}{\varphi} K_d + 1 \right) t \right] + \frac{C^s}{\varphi} K_d B_o \qquad (7.7)$$

where $B_o = \dfrac{C^d|_{t=0} + C^p|_{t=0}}{\dfrac{C^s}{\varphi} K_d + 1}$, and $A_o = C^d|_{t=0} - B_o$

In terms of dissolved concentration per unit volume of water the solution (7.6, 7.7) can be rewritten as

$$\varphi \hat{C}^d = A_o \exp\left[-a\left(\frac{C^s}{\varphi} K_d + 1 \right) t \right] + B_o \qquad (7.8)$$

$$C^p = -A_o \exp\left[-a\left(\frac{C^s}{\varphi} K_d + 1 \right) t \right] + \frac{C^s}{\varphi} K_d B_o \qquad (7.9)$$

where $B_o = \dfrac{\varphi \hat{C}^d|_{t=0} + C^p|_{t=0}}{\dfrac{C^s}{\varphi} K_d + 1}$, and $A_o = \varphi \hat{C}^d|_{t=0} - B_o$

Assuming equilibrium tracer distribution between solid and liquid phases the concentrations of the dissolved and particulate fractions can be found from

$$C^s K_d = \lim_{t \to \infty} \left(\frac{C^p}{\hat{C}^d} \right) \qquad (7.10)$$

$$\hat{C}^d \cdot \varphi + C^p = M = const \qquad (7.11)$$

Solving (7.10, 7.11) gives

$$\hat{C}^d = \frac{M}{C^s K_d + \varphi} \qquad (7.12)$$

$$C^p = M - \hat{C}^d \cdot \varphi \qquad (7.13)$$

Typical Kd values for ^{137}Cs and ^{90}Sr isotopes are 0.1 m^3/kg and 2 m^3/kg, respectively (Zheleznyak et al., 1992). Typical time scale for those radionuclides exchange between solid and liquid phases is 1 day.

In MECOSED sorption and desorption are calculated using either assumption of equilibrium distribution or solving equations for the sorption kinetics.

7.2 Decay

To allow for simulation of radioactive tracers (or other tracers with some first order loss), MECOSED incorporates a decay process. A tracer with the decay constant k will have its concentration C reduced at a rate given by

$$\frac{\partial C}{\partial t} = -kC \tag{7.14}$$

This can be solved analytically, so that the concentration after a time step dt is:

$$C(t+dt) = C(t)\exp(-k \cdot dt) \tag{7.15}$$

8 NUMERICAL IMPLEMENTATION

8.1 Numerical grid

Time-varying numerical grids can generate apparent material fluxes between the grid layers, introducing numerical diffusion. When this artificial diffusion is comparable or exceeds diffusion due to physical or biological processes, the predicted distribution of any property in water or in sediments will be distorted. Diffusion in sediments is typically orders of magnitude less intensive than mixing in surface water. Hence, extra care has to be exercised when choosing numerical grids for sediments. The numerical grid in sediments is also supposed to have high vertical resolution near the sediment-water interface, where the sediment and water properties often exhibit high gradients.

Stretched depth-adapted numerical grids are commonly used in atmospheric and ocean modelling to maintain high spatial resolution in areas of elevated variability of simulated fields (Phillips, 1957; Blumberg & Mellor, 1987). Numerical grids based on sigma coordinates, having thickness of grid layers scaled by water depth, provide an example of such grid configurations. Using notations introduced in Figure 1.1, a sigma grid ($\tilde{z}$) in sediments can be specified as follows:

$$\tilde{z}_{k-} = z_a + \sigma_{k-}(z_a - z_{bot}),\ z_a > \tilde{z}_{k-} \geq z_{bot} \tag{8.1}$$

$$\sigma_{k-} = \left(-\frac{z_a - \tilde{z}_{k-}}{z_a - z_{bot}} \right)_{t=t_0},\quad z_a > \tilde{z}_{k-} \leq z_{bot} \tag{8.2}$$

An evolution of the levels in this grid is illustrated in Figure 8.1a. The upper curve indicates location of the top level of the sediment grid, which coincides with the sediment water

interface and varies with time due to regular resuspension and deposition of sediments and due to gradual swelling of the seabed. Zero level denotes the location of the initial, undisturbed seabed surface. The sigma levels maintain refined resolution near the sediment-water interface throughout the simulation but, as shown later, they introduce large numerical diffusion in deep sediments. To reduce apparent fluxes, additional constraints must be imposed on the grid levels.

The following equation provides an example of a grid, which has reduced mobility of the grid levels under the top sediments:

$$\hat{z}_{k-} = \begin{cases} \min\left[(\hat{z}_{k+} - \Delta),\ \hat{z}_{k-}^{(n-1)}\right], & \dfrac{\partial z_a}{\partial t} < 0, \quad z_a > \hat{z}_{k-} \geq z_{bot} \\ \hat{z}_{k-}^{(n-1)}, & \dfrac{\partial z_a}{\partial t} \geq 0, \quad z_a > \hat{z}_{k-} \geq z_{bot} \end{cases} \tag{8.3}$$

Here Δ is a predefined minimum thickness of the sediment layers, and (n-1) denotes one time step back in time. For the sake of convenience in this paper we will refer to grid (8.3) as a k-grid. During the deposition event, this grid accommodates new sediments by varying only the top sediment layers. During the resuspension event, the grid layers in deep sediments remain immobilised until the erosion depth is large enough to reach this layer. The k-grid levels in deep sediments are less mobile than sigma-levels and hence less diffusive, however, as illustrated in Figure 8.1b, the k-grid fails to maintain a high vertical resolution of the top sediments during the deposition event.

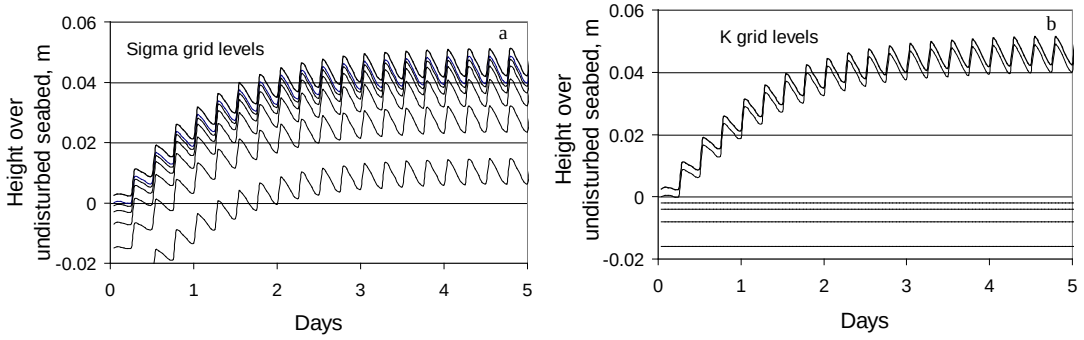

Figure 8.1. Stretched numerical grids (a) sigma grid (b) k-grid. Zero level represents initial location of the sediment-water interface.

To achieve both high vertical resolution in the top sediments and low numerical diffusion in deep layers, we combined the k-grid (17) and the sigma-grid (15) into a single k-sigma grid, which is defined as follows:

$$z_{k-} = \hat{z}_{k-} + p(\tilde{z}_{k-} - \hat{z}_{k-}),\ z_a > z_{k-} \geq z_{bot} \tag{8.4}$$

Here *p* is a weight coefficient varying from zero to one.

An evolution of the combined k-sigma grid levels is illustrated in Fig. 8.2. The sigma component of the grid adjusts the coordinate levels to long-term variations of the bathymetry, while the k-grid component enables the top sediment layer to follow high frequency oscillations of the sediment thickness. Varying the *p* value changes the time-scales of the grid relaxation to the sediment thickness. Increasing *p* freezes the deep sediment levels, reducing numerical diffusion in deep sediments and at the same time reducing resolution of the top sediments. Decreasing the *p* value improves the resolution of the top sediments, but tends to introduce higher numerical diffusion in deep layers.

From (8.4), the velocity of the grid levels can be calculated as $V_g = \partial z_{k-} / \partial t$.

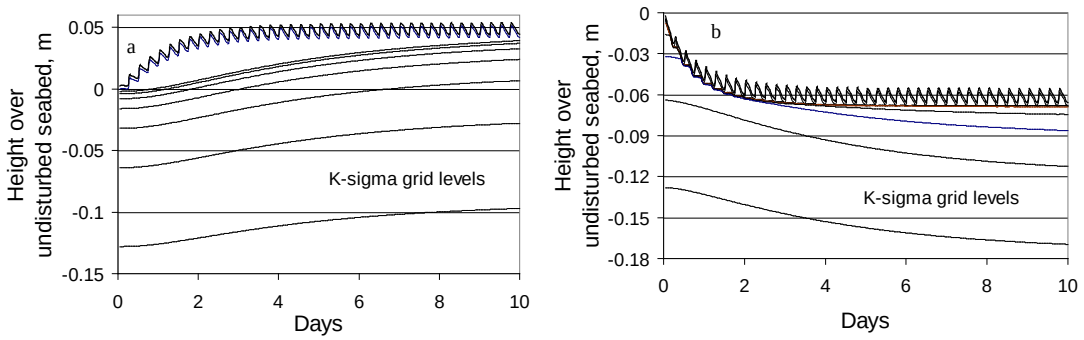

Figure 8.2. K-sigma grid levels in (a) erodible swelling (b) erodible consolidating sediments (p=1e-2). Zero level represents initial location of the sediment-water interface.

8.2 Simulation steps

Since the sediment transport is assumed to be independent from the transport of water and dissolved tracers, the model first solves equations for the sediment transport, then updates water flow and finally solves equations for the dissolved and sediment-attached material transport. The simulation steps are as follows:

(A) *Sediment transport*

Sediment concentration in water column

1. Calculate settling velocity of cohesive sediment and relative content of cohesive particles in a sediment bed.
2. Using expression for the sediment erosion/deposition/mixing fluxes find erosion flux and find coefficient for implicit representation of deposition flux.
2. Simulate diffusion, erosion, deposition and settling in water column.
3. Update erosion/deposition flux, using updated concentrations in water column. (this step is required as the deposition term was calculated implicitly).
4. If a net sediment flux is directed from the seabed into the water column (sediments are resuspended), check if there is enough amount of sediment in active layer.
5. If there are not enough particles in the top sediment layer transfer available amount of sediments from this layer into the water column. Set erosion and deposition fluxes to zero. Calculate diffusion and settling. Having known amount of sediment taken from an active layer, specify the erosion flux.

Sediment thickness

1. Calculate velocities of solid particles in a consolidating/swelling sediment bed.
2. Update sediment thickness and coordinate levels.
   2.1 Calculate location of the "water column – sediment bed" interface.
   2.2 Specify the thickness of an active layer.
   2.3 Specify grid levels.

Sediment concentration in a seabed

1. Calculate relative velocities of sediment particles.
2. Update sediment concentration in bed.
3. Update coordinate levels and concentrations in water column
4. Find porosity and update concentrations in water column and in sediment bed if porosity is less than predefined minimum value.

(B) Dissolved transport

1. Update water flow between layers.
2. Calculate concentrations
   2.1 If the water flow in directed from water column to sediment bed solve transport equations for water column first, using implicit representation for the tracers outflow.
   2.2 Update tracer fluxes at the water column – sediment bed interface
   2.3 Having known the tracer's influx update concentration in sediment bed using explicit representation for the influx.
   2.4 If the water flow in directed from sediment bed into the water column solve transport equation for the sediment bed first, using implicit representation for the tracers outflow.
   2.5 Calculate fluxes at the water column – sediment bed interface
   2.6 Having known the influx update concentration in water column using explicit representation for the influx.
3. Diffuse dissolved tracer across the "water column – sediment bed" interface

(C) Adsorbed tracer

1. Using sediment fluxes determined in (A), simulate diffusion, erosion, deposition and settling in water column.
2. Update erosion/deposition flux, using updated concentrations in water column. (this step is required as the deposition term was calculated implicitly).
3. If a net flux is directed from sediment bed into the water column (tracer is resuspended), check if there is enough amount of the tracer in active layer.
4. If there is no enough amount of the tracer in active layer transfer this tracer from an active layer into the water column. Set erosion and deposition fluxes to zero. Do diffusion and settling. Having known amount of sediments taken from an active layer, update erosion flux.
5. Calculate sorption/desorption exchanges between solid and liquid phases.

(D) Next time step

1. Repeat (A)

More details on numerical implementation of MECOSED can be found in Appendix B and C.

REFERENCES

1. Ambrose, R.B., Wool, T.A., Martin, J.L., 1993. The water quality analysis simulation program, WASP5 Part A: Model Documentation. Environmental Research Laboratory, Athens, Georgia 30613.
2. Ariathurai, R., Krone, R. B., 1976. Finite element model for cohesive sediment transport. J. Hydraul. Div. ASCE, 104, HY2, 323-328.
3. Black K.P., Oldman, J.W., 1999. Wave mechanisms responsible for grain sorting and non-uniform ripple distribution across two moderate-energy , sandy continental shelves. Marine Geology 162, 121-132.
4. Blumberg, A., Mellor, G., 1983. Diagnostic and prognostic numerical circulation studies of the South Atlantic Bight. J. of Geophysical Research 88, 4579-4592.
5. Boudreau B.P., 1997. Diagenetic Models and Their Implementation. Springer-Verlag, 414 p.
6. Boudreau B.P., 1997. A one-dimensional model for bed-boundary layer particle exchange. Journal of Marine Systems, 11, pp 279-303.
7. Cancino, L., Neves, R., 1999. Hydrodynamic and sediment suspension modelling in estuarine systems. Part I: Description of the numerical models. J. Marine Sys., 22, 105-116 pp.
8. Coastal Engineering Manual, Part III., 1999. U.S. Army Corps of Engineers. Washington, DC 20314-1000.
9. Dyer, K.R., 1989. "Sediment processes in estuaries: future research requirements". J. Geophys. Res., 94(C10), 14327-14339.
10. Delo, E.A., 1988. Estuarine muds manual. Tech. Rep. SR164, Hydraulic Res., Wallingford, England.
11. Glenn, S.M., Grant, W.D., 1987. A suspended sediment stratification correction for combined wave and current flows. J. Geophys. Res., 92(C8), 8244-8264 pp.
12. Gibson, R.E., England, G.L., Hussey, M.J.L., 1967. The theory of one-dimensional consolidation of saturated clays-I. Geotechnique 17, 261-73.
13. Govindaraju, R., Ramireddygari, R., Shrestha, P., Roig, L., 1999. Continuum bed model for estuarine sediments based on nonlinear consolidation theory. J. Hydrulic Engng. 125 (3), 300-304.
14. Grant, D., Madsen, O., 1982. Movable bed roughness in unsteady oscillatory flow. J. Geophys. Res., 87(C1), 469-481 pp.
15. Grant, D., Madsen, O., 1986. The continental shelf bottom boundary layer. Ann. Rev. Fluid Mech. 18, p 265-305.
16. Harris, C., Wiberg, P., 2001. A two-dimensional, time-dependent model of suspended sediment transport and bed reworking for continental shelves. Computers and Geoscience 27, 675-690.
17. Howes, T., 2002. Riverine turbidity processes. Final report No RT1.5 for SEQRWQMS, 128 p.
18. Jankowski, J.A., Malcherek, A., Zielke, W., 1996. Numerical modelling of suspended sediment due to deep-see mining. J. Geophys. Res., 101(C2), 3545-3560.
19. Li, Z.H., Ngyen, K.D., Brun-Cottan, J.C., Martin J.M., 1994. Numerical simulation of the turbidity maximum transport in Gironde estuary (France). Oceanologica Acta.
20. Li, M., Amos, C., 2001. SEDTRANS96: the upgraded and better calibrated sediment-transport model for continental shelves. Computers and Geoscience 27, 619-645.
21. Madsen, O.S., 1994. Spectral wave-current bottom boundary layer flows, in Coastal Engineering 1994 Proceedings, 24th international conference Coastal Engineering Research Council/ASCE, pp. 384-398.
22. Margvelashvili, N., Maderich, V., and Zheleznyak, M., 1997. THREETOX - a computer code to simulate three-dimensional dispersion of radionuclides in stratified water bodies. Radiation Protection Dosimetry, Nuclear Technology Publishing, Vol. 73, Nos 1-4, pp. 177-180.

23. Margvelashvili, N., 2009. Stretched Eulerian coordinate model for coastal sediment transport. Computers and Geosciences, 35, 1167-1176.
24. Mehta, A., Hayter, W., Parker, R., Krone, R., Teeter, A., 1989. Cohesive sediment transport. 1: Process description. J. Hyd. Engng., 115, 1076-1093.
25. Mitchener, H., Torfs, H., 1996. Erosion of mud/sand mixtures. Coastal Engineering 29, 1-25.
26. Onishi, Y., Dummuller, D.C., Trent, D.S., 1989. Preliminary Testing of Turbulence and Radionuclide Transport Modeling in Deep Ocean Environment. PNL-6853, Pacific Northwest Laboratory, Richland, Washington.
27. Onishi, Y., Serne, J., Arnold, E., Cowan, C., Thompson, F., 1981. Critical review: radionuclide transport, sediment transport, water quality, mathematical modelling and radionuclide adsorption/desorption mechanism. NUREG/CR-1322, Pacific Northwest Laboratory, Richland, 512 pp.
28. Partheniades, E., 1965. Erosion and deposition of cohesive soils. J.Hydraul.Div. ASCE 91, p. 105-139.
29. Phillips, N.A., 1957. A coordinate system having some special advantages for numerical forecatsting. J. of Meteorology 14, 184-185.
30. Reed, C.W., Neidoroda, A.W., Swift, D.J.P., 1999. Modelling sediment entrainment and transport processes limited by bed armoring. Marine Geology 154, pp 143-154.
31. Smith, J.D., McLean, S.R., 1977. Spatially averaged flow over a wavy bed. J. Geophys. Res., 82, 1735-1746.
32. Shrestha, P.A., Orlob, G.T., 1989. Multiphase distribution of cohesive sediments and heavy metals in estuarine systems. J. Environ. Engrg., 122, 730-740.
33. Swart, D.H., 1974. Offshore Sediment Transport and Equilibrium Beach Profiles. Publication no. 131, Delft Hydraulics Laboratory, Delft, The Netherlands.
34. Thomas, D.N., Judd, S.J., Fawcett, N., 1999. Flocculation modelling: a review. Wat. Res., 33 (7), pp. 1579-1592.
35. Toorman, E., 1996. Sedimentation and self weight consolidation: general unifying theory. Geotechnique 46 (1), 103-113.
36. Torfs, H., Mitchener, H., Huysentruy, H., Toorman, E., 1996. Settling and consolidation of muf/sand mixtures. Coastal Engineering 29, 27-45.
37. Uncles, R.J., Stephens, J.A., 1989. Distribution of suspended sediment at high water in a macrotidal estuary. J. Geophys. Res., 94(C10), 14395-14405.
38. Walker S.J., Sherwood C.R. A transport model of Port Phillip Bay. CSIRO, Division of Oceanography, Technical Report N 39, 1997, p.59.
39. Wiberg, P.L., Harris, C.K., 1994. Ripple geometry in wave-dominated environments. J. Geophys. Res. 99, 775-789.
40. Wiberg, P.L., Rubin, D.M., 1989. Bed roughness produced by saltating sediments. J. Geophys. Res., 94, 5011-5016.
41. Wikramanayake, P.N., 1993. Velocity profiles and suspended sediment transport in wave-current flows. Ph.D. dissertation, MIT, 285pp.
42. Winterwerp, J.C., 1998. A simple model for turbulence induced flocculation of cohesive sediment. J. Hydraulic Res., 36 (3), pp 309-326.
43. Winterwerp, J.C., Cornelisse, J.M., Kuijper, C., 1991. The behaviour of mud from Western Sceldt under tidal conditions. Delft Hydraulics, The Netherlands, Rep. Z161-37/HW/paper1.wm, 14 pp.
44. Van Rijn, L.C., 1984a. Sediment transport, Part I: Bed load transport. J. Hydraul.Engineering 110, 1431- 1456.
45. Van Rijn, L.C., 1984b. Sediment transport, Part II: Suspended load transport. J. Hydraul.Engineering 110, 1613- 1641.
46. Van Rijn, L.C., 1993. Principles of sediment transport in Rivers, Estuaries and Coastal Seas. Aqua Publication, Amsterdam (multiply pagination).
47. Zheleznyak, M., Demchenko, R., Khursin, S., Kuzmenko, Yu., Tkalich, P., Votiuk, N., 1992. Mathematical modelling of radionuclide dispersion in the Pripyat-Dnieper aquatic system after the Chernobyl accident. The Science of Total Environment 112, 89-14.

48. You, B. et al. 1999. Task Resuspension Dynamics (RD) Phase 2 Final Report. Southeast Queensland Water Quality Strategy, 81 p.

Appendix A: Mass balance equations

In an Eulerian immobilised coordinate frame z, a general mass balance equation for the particulate or dissolved tracer can be expressed as follows (Boudreau, 1997):

$$\frac{\partial \varphi C}{\partial t} + \frac{\partial (\varphi C U)}{\partial z} = \frac{\partial}{\partial z}\left(\varphi \nu \frac{\partial C}{\partial z}\right) \tag{A1}$$

Here C is either the volumetric concentration of the particulate tracer or concentration of the dissolved tracer in pore water, U is the material velocity given in a time-invariant coordinate frame, and φ is the porosity when C is a dissolved tracer and $\varphi \equiv 1$ when (1) is applied to a particulate fraction.

Introducing a new set of independent variables

$$t^* = t;\ z^* = z^*(t);\ \frac{\partial z^*}{\partial z} = 1 \tag{A2}$$

and applying a chain rule to link derivatives in the old system to those in the new system

$$\frac{\partial \varphi C}{\partial t} = \frac{\partial \varphi C}{\partial t^*} + \frac{\partial \varphi C}{\partial z^*}\frac{\partial z^*}{\partial t};\ \frac{\partial \varphi C}{\partial z} = \frac{\partial \varphi C}{\partial z^*} \tag{A3}$$

the mass balance equation (A1) is transformed into:

$$\frac{\partial \varphi C}{\partial t^*} + \frac{\partial \varphi C}{\partial z^*}\frac{\partial z^*}{\partial t} + \frac{\partial \varphi C U}{\partial z^*} = \frac{\partial}{\partial z^*}\left(\varphi \nu \frac{\partial C}{\partial z^*}\right), \tag{A4}$$

After a number of manipulations involving expansion of partial derivatives and combining different terms, (A4) can be transformed to

$$\frac{\partial \varphi C}{\partial t^*} + \frac{\partial}{\partial z^*}\left[\varphi\left(\frac{\partial z^*}{\partial t} + U - \nu \frac{\partial}{\partial z^*}\right)C\right] - \varphi C \frac{\partial}{\partial z^*}\left(\frac{\partial z^*}{\partial t}\right) = 0 \tag{A5}$$

Introducing the velocity of new coordinate levels as seen by an observer in an immobilised coordinate system (note that $\partial z^* / \partial t$ is velocity of the old frame points with regard to new coordinate levels):

$$V_g = -\frac{\partial z^*}{\partial t}, \tag{A6}$$

and suppressing the star superscripts in the notation of the independent variables, equation for the mass conservation in a time-varying coordinate frame can be expressed as:

$$\frac{\partial \varphi C}{\partial t} = -\frac{\partial}{\partial z}\left[\varphi\left(\tilde{U} - \nu \frac{\partial}{\partial z}\right)C\right] - \varphi C \frac{\partial V_g}{\partial z} \tag{A7}$$

Here $\tilde{U} = U - V_g$ is the material velocity expressed in a time-varying frame

Assuming C=1, and zero diffusion coefficient in (A7) gives a mass conservation equation for the liquid phase

$$\frac{\partial \varphi}{\partial t} + \frac{\partial \left(\varphi \tilde{U}^w\right)}{\partial z} + \varphi \frac{\partial V_g}{\partial z} = 0 \qquad \text{(A8)}$$

Equation for the concentration of solids reads

$$\frac{\partial C}{\partial t} = -\frac{\partial}{\partial z}\left[\left(\tilde{U} - \nu \frac{\partial}{\partial z}\right)C\right] - C\frac{\partial V_g}{\partial z} \qquad \text{(A9)}$$

Having sediment represented by single class of particles: $\frac{C}{\rho} = (1-\varphi)$, and dividing the left and right hand side of (A9) by the sediment density, and neglecting diffusion, transforms (A9) into

$$\frac{\partial (1-\varphi)}{\partial t} + \frac{\partial \left[(1-\varphi)\tilde{U}\right]}{\partial z} + (1-\varphi)\frac{\partial V_g}{\partial z} = 0 \qquad \text{(A10)}$$

Introducing a time-varying coordinate frame $V_g = U$, and substituting in (A10) porosity by void ratio $(1-\varphi) = \frac{1}{(1+\varepsilon)}$, reduces (A10) to

$$\frac{\partial \varepsilon}{\partial t} = (1+\varepsilon)\frac{\partial U}{\partial z}. \qquad \text{(A11)}$$

Using the expression for the sediment velocity in a cohesive consolidating sediment (Toorman, 1996)

$$U = -\frac{K_h}{g\rho^w}\left(\frac{\partial \sigma_e}{\partial \varepsilon}\right)\frac{\partial \varepsilon}{\partial z} - \frac{K_h}{(1+\varepsilon)}\frac{(\rho^s - \rho^w)}{\rho^w} \qquad \text{(A12)}$$

and introducing new coordinates $\frac{\partial \xi}{\partial z} = \frac{1}{1+\varepsilon}$, transforms (A11) to the finite strain consolidation equation derived by Gibson et al. (1967)

$$\frac{\partial \varepsilon}{\partial t} = \frac{\partial}{\partial \xi}\left[-\frac{K_h}{(1+\varepsilon)g\rho^w}\left(\frac{\partial \sigma_e}{\partial \varepsilon}\right)\frac{\partial \varepsilon}{\partial \xi} - \frac{K_h}{(1+\varepsilon)}\frac{(\rho^s - \rho^w)}{\rho^w}\right] \qquad \text{(A13)}$$

Here σ_e is an effective stress, and K_h is hydraulic conductivity.

Appendix B: Finite-difference approximation

A general form of the calculated advection-diffusion equation is

$$\frac{\partial}{\partial t}\left(C\cdot\varphi\cdot Z\right)_k = -\partial_z\left[\varphi\left(U-\nu\frac{\partial}{\partial z}\right)C\right]_k \qquad \text{(B 1)}$$

with the boundary conditions specified at the top and the bottom boundaries

$$\left(U-\nu\frac{\partial}{\partial z}\right)\cdot C = F_{bot/in}+F_{bot/out}, \quad z=z_{bot} \qquad \text{(B 2)}$$

$$\left(U-\nu\frac{\partial}{\partial z}\right)\cdot C = F_{top/in}+F_{top/out}, \quad z=z_{top} \qquad \text{(B 3)}$$

Here z_{bot} and z_{top} are the bottom and the top boundaries of the layer, respectively. z coordinate is directed upward. $F_{bot/out} <= 0$ denotes material fluxes out of the modelling domain through the bottom boundary; $F_{bot/in} > 0$ is material influx into the computational domain through the bottom boundary, $F_{top/out} > 0$ is material flux out of the modelling domain through the surface boundary, and $F_{top/in} <= 0$ is surface influx. The description of indexes follows notations introduced in figure 1.

The governing equations (B1-B3) are transformed to the system of three-diagonal, algebraic equations, which is solved using Thompson's method [ ]. The coefficients of the algebraic equations are defined using the following finite difference representation

In the interior of the water column or in sediment bed: k=/=kbot, k=/=ktop

$$\frac{\left(C_k\cdot\varphi_k\cdot Z_k\right)}{\Delta t}+(\varphi UC)_{k+}-(\varphi UC)_{k-}-\left(\varphi_{k+}\nu_{k+1}\frac{C_{k+1}-C_k}{Z_{k+}}\right)+\left(\varphi_{k-}\nu_k\frac{C_k-C_{k-1}}{Z_{k-}}\right)= \qquad \text{(B 4)}$$
$$=\frac{\left(C_k\cdot\varphi_k\cdot Z_k\right)^{(n-1)}}{\Delta t}$$

$$(\varphi UC)_{k+}=\begin{cases}(\varphi_{k+1}U_{k+1}C_{k+1}), & U_{k+1}<=0\\ (\varphi_k U_{k+1}C_k), & U_{k+1}>0\end{cases} \qquad \text{(B 5)}$$

$$(\varphi UC)_{k-}=\begin{cases}(\varphi_k U_k C_k), & U_k<=0\\ (\varphi_{k-1}U_k C_{k-1}), & U_k>0\end{cases} \qquad \text{(B 6)}$$

At the bottom boundary: k=kbot

$$\frac{(C_k \cdot \varphi_k \cdot Z_k)}{\Delta t} + (\varphi UC)_{k+} - \left(\varphi_{k+} \nu_{k+1} \frac{C_{k+1} - C_k}{Z_{k+}}\right) - \left(\frac{F_{bot/out}}{C_k^{(n-1)}}\right) C_k = \\ = \frac{(C_k \cdot \varphi_k \cdot Z_k)^{(n-1)}}{\Delta t} + F_{bot/in} \qquad \text{(B 7)}$$

$$F_{bot/in} + F_{bot/out} = (\varphi UC)_{k-} - \left(\varphi_{k-} \nu_k \frac{C_k - C_{k-1}}{Z_{k-}}\right) \qquad \text{(B 8)}$$

At the surface boundary: k=ktop

$$\frac{(C_k \cdot \varphi_k \cdot Z_k)}{\Delta t} - (\varphi UC)_{k-} + \left(\varphi_{k-} \nu_k \frac{C_k - C_{k-1}}{Z_{k-}}\right) + \left(\frac{F_{top/out}}{C_k^{(n-1)}}\right) C_k = \\ = \frac{(C_k \cdot \varphi_k \cdot Z_k)^{(n-1)}}{\Delta t} - F_{top/in} \qquad \text{(B 9)}$$

$$F_{top/in} + F_{top/out} = (\varphi UC)_{k+} - \left(\varphi_{k+} \nu_{k+1} \frac{C_{k+1} - C_k}{Z_{k+}}\right) \qquad \text{(B 10)}$$

Here $\varphi_{k+} = 0.5(\varphi_k + \varphi_{k+1})$, $\varphi_{k-} = 0.5(\varphi_{k-1} + \varphi_k)$, $Z_{k+} = 0.5(Z_k + Z_{k+1})$, and $Z_{k-} = 0.5(Z_{k-1} + Z_k)$. Boundary fluxes in (B8, B10) are specified through the corresponding boundary conditions.

Appendix C: Simulation steps

(Simulation steps shown in this appendix do not include diffusion across water sediments and transport of the sediment-attached tracers).

Since the sediment transport is assumed to be independent from the transport of water and dissolved tracers, the model first solves equation for sediment transport, then updates water flow and finally solves equation for the dissolved material transport. The simulation steps are as follows:

(A) The model updates settling velocity of the suspended sediments and solves advection diffusion equation for suspended sediment concentration expressed in a conservative form

$$\frac{\partial}{\partial t}\left(C_i^s \cdot Z\right)_k = -\partial_z\left[\left(\tilde{U}_i^s - \nu_i^s \frac{\partial}{\partial z}\right)\cdot C_i^s\right]_k . \qquad \text{(C1)}$$

Boundary conditions are given by

$$\left(\tilde{U}_i^s - \nu_i^s \frac{\partial}{\partial z}\right)\cdot C_i^s = 0; \qquad z = z_{top} \qquad \text{(C2)}$$

$$\left(\tilde{U}_i^s - \nu_i^s \frac{\partial}{\partial z}\right)\cdot C_i^s = Q_i^s; \qquad z = z_{\text{int}} \qquad \text{(C3)}$$

and operator $\partial_z(f)_k$ is defined as $\partial_z(f)_k = f_{(k+)} - f_{(k-)}$.

During this step, the numerical grid remains immobilised and both $C_{i,k}^s$ and Z_k are known from the previous time-step. The finite difference scheme is implicit with respect to suspended sediment concentration in the right hand side of (C1). The boundary conditions include implicit representation for the settling terms, and explicit representation for the sediment resuspension terms. Due to implicit representation of the boundary conditions, actual amount of resuspended sediments is known only after solution of (C1-C3). If there is no sufficient amount of sediments in a sea bed, then the model reduces the resuspension fluxes to the amount of sediments available in the top sediment layer, and repeats solution of (C1-C3).

(B) Next step is to define velocity of consolidating particles in a seabed by solving first order ordinary differential equation

$$\frac{\partial U_c^s}{\partial z} \approx \frac{1}{(1+\varepsilon)}\frac{(\varepsilon - \varepsilon_m)}{T_c}, \qquad \text{(C4)}$$

with the following boundary condition at the bottom of the benthic layer

$$U_c^s = 0; \qquad z = z_{bot} \qquad \text{(C5)}$$

(C) Once the sediment fluxes across the sediment-water interface and velocity of consolidating particles are known from (A) and (B) steps, the model updates the sediment thickness and grid layers in sediments solving equation for the seabed-water interface location

$$\frac{\partial z_{\text{int}}}{\partial t} = U_c^{\ s}\,|_{z=z\,\text{int}} - \sum_{i=1}^{n}(1+\varepsilon_{i,w/b})\frac{Q_i^{\ s}}{\rho_i^{\ s}}, \qquad \text{(C6)}$$

and updating the numerical grid layers according to the grid equations ( ).

(D) Having known sediment fluxes across water-seabed interface and having updated grid levels in sediments, the model solves advection-diffusion equations for the seabed particles

$$\frac{\partial}{\partial t}\left(C_i^{\ s}\cdot Z\right)_k = -\partial_z\left[\left(\tilde{U}_i^{\ s} - \nu_i^{\ s}\frac{\partial}{\partial z}\right)\cdot C_i^{\ s}\right]_k \qquad \text{(C7)}$$

with the boundary conditions

$$\left(\tilde{U}_i^{\ s} - \nu_i^{\ s}\frac{\partial}{\partial z}\right)\cdot C_i^{\ s} = 0; \qquad z = z_{bot} \qquad \text{(C8)}$$

$$\left(\tilde{U}_i^{\ s} - \nu_i^{\ s}\frac{\partial}{\partial z}\right)\cdot C_i^{\ s} = Q_i^{\ s}; \qquad z = z_{\text{int}} \qquad \text{(C9)}$$

Equations (C7-C9) are similar to (C1-C3), except that sediment fluxes across the water-sediment interface, shown in the right-hand side of (C9), now are known from step (A).

(E) The model updates numerical grid and sediment concentrations in water column (since the sediment thickness has been updated in step C), and updates porosity in water and in sediments.

This ends one time-step simulation of sediment transport, and the model proceeds with calculating dissolved material transport.

(F) By this time, the numerical grid and porosity in benthic and pelagic layers have been updated, and the model can calculate water velocities from the mass conservation equation expressed in a conservative form

$$-\partial_z\left[\varphi\tilde{U}^{w}\right]_k = \frac{\partial}{\partial t}\left(\varphi Z\right)_k \qquad \text{(C10)}$$

$$\varphi\tilde{U}^{w} = 0; \qquad z = z_{bot} \qquad \text{(C11)}$$

(G) Having this done, the concentration of the dissolved material in water and in sediments is updated from the mass conservation equation

$$\frac{\partial}{\partial t}\left(C_i^{\ d}\cdot\varphi\cdot Z\right)_k = -\partial_z\left[\varphi\left(\tilde{U}^{w} - \nu_i^{\ d}\frac{\partial}{\partial z}\right)C_i^{\ d}\right]_k \qquad \text{(C12)}$$

Boundary conditions are given by

$$\varphi\left(\tilde{U}^{w} - \nu_i^{\ d}\frac{\partial}{\partial z}\right)\cdot C_i^{\ d} = 0; \qquad z = z_{top}, \quad z = z_{bot} \qquad \text{(C13)}$$

$$\varphi\left(\tilde{U}^{w} - \nu_i^{d}\frac{\partial}{\partial z}\right)\cdot C_i^{d} = \varphi F^{w}\cdot C_{i,w/b}{}^{d}; \qquad z = z_{int} \qquad \text{(C14)}$$

Having completed this simulation cycle, the model proceeds further with the next time step starting with (A).

Appendix D: Diffusion across water-sediment interface

Diffusion of solid tracers across the water-sediment interface is calculated simultaneously with the resuspension and deposition using finite difference approximations. Diffusion of the dissolved tracers between water and sediment bed, for the sake of simplicity of the code, is calculated using analytical solution. Dissolved mixing across water and sediment bed is determined from the solution of the equations:

$$\begin{cases} \dfrac{\partial}{\partial t}\left(\Delta Z \varphi C^{d}\right)_{wc} = -\nu_{o} \dfrac{C_{wc}^{\ d} - C_{bed}^{\ d}}{\min(\Delta Z_{wc}, \Delta Z_{bed})} \min(\varphi_{wc}, \varphi_{bed}) \\ \dfrac{\partial}{\partial t}\left(\Delta Z \varphi C^{d}\right)_{bed} = \nu_{o} \dfrac{C_{wc}^{\ d} - C_{bed}^{\ d}}{\min(\Delta Z_{wc}, \Delta Z_{bed})} \min(\varphi_{wc}, \varphi_{bed}) \end{cases} \quad \text{(D1)}$$

These equations represent the boundary condition for the dissolved tracers given in terms of point sources rather then fluxes. Introducing new variables

$$M_{wc} = \left(\Delta Z \varphi C^{d}\right)_{wc}, \quad M_{bed} = \left(\Delta Z \varphi C^{d}\right)_{bed} \quad \text{(D 2)}$$

equation (D 1) can be rewritten as

$$\begin{cases} \dfrac{\partial M_{wc}}{\partial t} = -(RM_{wc} - DM_{bed}) \\ \dfrac{\partial M_{bed}}{\partial t} = (RM_{wc} - DM_{bed}) \end{cases} \quad \text{(D 3)}$$

where $R = \nu_{o} \dfrac{\min(\varphi_{wc}, \varphi_{bed})}{\Delta Z_{wc} \varphi_{wc} \min(\Delta Z_{wc}, \Delta Z_{bed})}$, $D = \nu_{o} \dfrac{\min(\varphi_{wc}, \varphi_{bed})}{\Delta Z_{bed} \varphi_{bed} \min(\Delta Z_{wc}, \Delta Z_{bed})}$

An analytical solution of (D 3) is:

$$M_{wc} = A_{o} \exp\left[-a(R+D)t\right] + DB_{o} \quad \text{(D 4)}$$

$$M_{bed} = -A_{o} \exp\left[-a(R+D)t\right] + RB_{o} \quad \text{(D 5)}$$

where $B_{o} = \dfrac{M_{wc}|_{t=0} + M_{bed}|_{t=0}}{R+D}$, and $A_{o} = M_{wc}|_{t=0} - DB_{o}$

Finally the concentrations are found from

$$C_{wc}^{\ d} = M_{wc} / (\Delta Z \varphi)_{wc}, \quad C_{bed}^{\ d} = M_{bed} / (\Delta Z \varphi)_{bed} \quad \text{(D 6)}$$

Appendix E: Reference concentrations

Assuming that a net flux (I_1) of sediments, suspended in a turbulent flow, is established as a balance between settling and turbulent diffusion, the concentration of suspended particles can be evaluated from

$$K\frac{\partial C}{\partial z} + w_g C = I_1 \tag{2}$$

where C is the sediment concentration, Wg is velocity of the sediment settling in a still water, K is diffusion coefficient.
Neglecting z-dependence for I_1, and substituting expression for vertical diffusion coefficient

$$K = \kappa u_* z + K_0 \tag{3}$$

in (2) and solving then that equation, gives the following general expression for the vertical profile of the sediment concentration

$$C = I_2 \cdot (z+\delta)^{-\delta\gamma} + \frac{I_1}{w_g}, \qquad \delta\gamma \neq 1 \tag{4}$$

$$C = \frac{I_2}{z+\delta} + \frac{I_1}{w_g}, \qquad \delta\gamma = 1 \tag{5}$$

Here $\gamma = \frac{w_g}{K_0}$ (1/m), $\delta = \frac{K_0}{\kappa u_*}$ (m), K_0 is the diffusivity coefficient in a viscous sublayer, κ is van Karman constant, u_* is shear velocity, and I1 I2 are integration constants.

Having the diffusion coefficient expressed in new variables

$$K = K_0\left(1+\frac{z}{\delta}\right), \tag{6}$$

shows that the parameter delta can be treated as the length scale of the viscous sub-layer.
The integration constants in (4, 5) can be defined using data for the total mass of sediment in the near bottom cell $M = C_0 \cdot D$, where D is the height of the near bottom computational cell, and the data for sediment concentration C_1 at the height H above the bed:

$$\delta\gamma \neq 1: \qquad C = C_1 = I_2 \cdot (H+\delta)^{-\delta\gamma} + \frac{I_1}{w_g}, \qquad z = H, \tag{7}$$

$$\delta\gamma \neq 1: \qquad M = \int_0^D C dz = I_2 \frac{(D+\delta)^{(1-\delta\gamma)} - \delta^{(1-\delta\gamma)}}{(1-\delta\gamma)} + \frac{I_1}{w_g} D, \tag{8}$$

$$\delta\gamma = 1: \qquad C = C_1 = \frac{I_2}{H+\delta} + \frac{I_1}{w_g}, \quad z = H \tag{9}$$

$$\delta\gamma = 1: \qquad M = I_2 \ln\left(\frac{D+\delta}{\delta}\right) + \frac{I_1}{w_g} D \tag{10}$$

From (7-10) the integration constants and vertical profile for the sediment concentration can be derived:

$$\delta\gamma \neq 1: \qquad I_2 = \frac{D(C_0 - C_1) p \delta^p}{1 - \left(\frac{\delta}{D+\delta}\right)^p - p\left(\frac{D}{H+\delta}\right)\left(\frac{\delta}{H+\delta}\right)^p} \tag{11}$$

$$\delta\gamma \neq 1: \qquad C(z_0) = I_2 \left(\left(\frac{1}{z_0+\delta}\right)^{p+1} - \left(\frac{1}{H+\delta}\right)^{p+1} \right) + C_1 \tag{12}$$

where $p = -(1-\delta\gamma) \neq 0$, $\delta = \frac{K_0}{\kappa u_*}$, $\gamma = \frac{w_g}{K_0}$

$$\delta\gamma = 1: \qquad I_2 = \frac{D(C_0 - C_1)}{\ln\left(\frac{D+\delta}{\delta}\right) - \frac{D}{H+\delta}} \tag{13}$$

$$\delta\gamma = 1: \qquad C(z_0) = I_2 \left(\frac{1}{z_0+\delta} - \frac{1}{H+\delta} \right) + C_1 \tag{14}$$

For numerical computations it is more convenient to express (11-12) as follows

$$\delta\gamma \neq 1: \qquad \frac{I_2}{\delta^p} = \frac{D(C_0 - C_1) p}{1 - \left(\frac{\delta}{D+\delta}\right)^p - p\left(\frac{D}{H+\delta}\right)\left(\frac{\delta}{H+\delta}\right)^p} \tag{11'}$$

$$\delta\gamma \neq 1: \qquad C(z_0) = \frac{I_2}{\delta^p} \left[\left(\frac{1}{z_0+\delta}\right)\left(\frac{\delta}{z_0+\delta}\right)^p - \left(\frac{1}{H+\delta}\right)\left(\frac{\delta}{H+\delta}\right)^p \right] + C_1 \tag{12'}$$

When I1=0, the reference concentration becomes

$$\delta\gamma \neq 1: \qquad \frac{I_2}{\delta^p} = \frac{DC_0 p}{1-\left(\frac{\delta}{D+\delta}\right)^p} \tag{11''}$$

$$\delta\gamma \neq 1: \qquad C(z_0) = \frac{I_2}{\delta^p}\left(\frac{1}{z_0+\delta}\right)\left(\frac{\delta}{z_0+\delta}\right)^p \tag{12''}$$

$$\delta\gamma = 1: \qquad I_2 = \frac{DC_0}{\ln\left(\frac{D+\delta}{\delta}\right)} \tag{13''}$$

$$\delta\gamma = 1: \qquad C(z_0) = I_2\left(\frac{1}{z_0+\delta}\right) \tag{14''}$$

In the case of constant vertical diffusion coefficient

$$K = K_0 = const\,, \tag{15}$$

solution of (2) is

$$C = I_2 \exp\left(-\frac{w_g}{K_0} z\right) + \frac{I_1}{w_g} \tag{16}$$

and the integration constants can be determined from the following expressions

$$C_1 = I_2 \exp(-\gamma H) + \frac{I_1}{w_g}, \qquad z = H \tag{17}$$

$$M = \frac{I_2}{\gamma}(1-\exp(-\gamma D)) + \frac{I_1}{w_g} D \tag{18}$$

From (16-18) the solution can be expressed as

$$I_2 = \frac{\gamma D(C_0 - C_1)}{1-\exp(-\gamma D) - \gamma D \exp(-\gamma H)} \tag{19}$$

$$C(z_0) = I_2(\exp(-\gamma z_0) - \exp(-\gamma H)) + C_1 \tag{20}$$

When the vertical gradient of sediment concentration in the near bottom area is high, and the thickness of the sediment layer, which is to be deposited within the computational time step (d = w * dt), is less than the thickness of the near bottom computational cell, the

solution becomes grid dependant, because the portion of the sediment profile that should be deposited is not resolved. To estimate deposition flux analytical expression for the vertical profile of the sediment concentration in the near bottom computational cell can be used. Integrating equations (12, 14, 19) from zero to the distance d gives the following expressions for deposited masses of sediment:

$$K = K_0\left(1+\frac{z}{\delta}\right)$$

$$m = \int_0^d C_0(z)dz = \frac{I_2}{p\delta^p}\left[1-\left(\frac{\delta}{d+\delta}\right)^p - p\frac{d}{(H+\delta)}\left(\frac{\delta}{H+\delta}\right)^p\right] + dC_1,\ p = -(1-\delta\gamma) \neq 0$$

(21)

where $I_2 = \dfrac{D(C_0 - C_1)p\delta^p}{1-\left(\dfrac{\delta}{D+\delta}\right)^p - p\left(\dfrac{D}{H+\delta}\right)\left(\dfrac{\delta}{H+\delta}\right)^p}$.

$$m = \int_0^d C_0(z)dz = I_2\left[\ln\left(\frac{d+\delta}{\delta}\right)-\left(\frac{d}{H+\delta}\right)\right] + C_1 d,\qquad p = -(1-\delta\gamma) = 0 \qquad (22)$$

where $I_2 = \dfrac{D(C_0 - C_1)}{\ln\left(\dfrac{D+\delta}{\delta}\right)-\dfrac{D}{H+\delta}}$.

$$K = K_0 = const$$

$$m = \int_0^d C_0(z)dz = \frac{I_2}{\gamma}\left[1-\exp(-\gamma d)-\gamma d\exp(-\gamma H)\right] + C_1 d, \qquad (23)$$

where $I_2 = \dfrac{\gamma D(C_0 - C_1)}{1-\exp(-\gamma D)-\gamma D\exp(-\gamma H)}$.

Appendix F: Velocity of sediment particles in stretching media

Volumetric changes in a consolidating column of the mixture of incompressible solid particles and incompressible water, with the sediment velocities at the top and bottom levels given by U1 and U2 (fig. F1), can be expressed as

$$(V_2 - V_1) = S(U_a - U_b)\Delta t \ , \qquad \text{(F1)}$$

where V_2 and V_1 are total (sediment and pore water) initial and final volumes, Δt is time interval, and S is an area of the horizontal cross-section of the column.

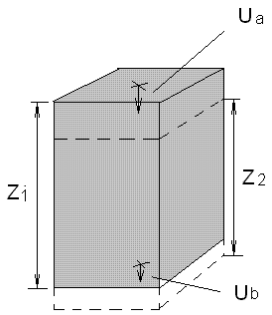

Fig. F1 Schematic diagram of consolidating sediment column

Dividing left and right hand sides of (F 1) by sediment volume (V^s) and time interval, and taking into account that the sediment volume in the column does not change, so that $V_2 - V_1 = V_2{}^w - V_1{}^w$, equation (F 1) can be rewritten as

$$\frac{V_2{}^w - V_1{}^w}{V^s \Delta t} = \frac{S(U_a - U_b)}{V^s} \qquad \text{(F 2)}$$

Using expression for void ratio ($\varepsilon = \frac{V^w}{V^s}$) and multiplying the denominator and the divisor in the right hand side of (F 2) by the column thickness Z_1 gives

$$\frac{\varepsilon_2 - \varepsilon_1}{\Delta t} = \frac{(U_a - U_b)SZ_1}{V^s Z_1} \qquad \text{(F 3)}$$

Substituting $\frac{SZ_1}{V^s}$ by $(1+\varepsilon)$, and approaching time interval Δt and the column thickness Z_1 to zero gives continuum form of the equation (F 3)

$$\frac{\partial \varepsilon}{\partial t} = \frac{\partial U}{\partial z}(1+\varepsilon) \qquad \text{(F 4)}$$

Appendix G: Table of notations

$(*)^s$ solid phase variable

$(*)^w$ liquid phase variable

$(*)^d$ dissolved tracer

$(*)^p$ tracer adsorbed by sediment

$C^s_{i,k}$ concentration of the i-th fraction of solid tracer [kg/(m^3 mixture)] (i=1,n)

$C^d_{j,k}$ concentration of the j-th dissolved tracer [kg/(m^3 water)] (j=1,m), and the

$C^p_{ji,k}$ concentration of the j-th tracer attached to the I-th fraction of sediment [kg/(m^3 mixture)] (j=1,l)

Z_k thickness of sediment or water column layer (m)

$z_{(k+)}$ coordinate of the upper level of the k-th layer (m)

$z_{(k-)}$ coordinate of the bottom level of the k-th layer (m)

V^w water volume

V^s_i volume of the I-th solid fraction

$V^s = \sum_{i=1}^{n} V^s_i$ total solid volume

$\varepsilon = \left(\frac{V^w}{V^s} \right)$ void ratio $\sum_{i=1}^{i=n} \frac{C^s_i}{\rho^s_i} = \frac{1}{1+\varepsilon}$.

$\varphi \equiv 1$ when it appears in a mass balance equation for sediments and sediment attached tracers

$\varphi = \frac{V^w}{V^s + V^w} = \frac{\varepsilon}{1+\varepsilon}$ porosity

ρ^w water density [kg/(m^3 water)]

ρ^s_i sediment density [kg/(m^3 solid)]

U^s_i velocity of the i-th fraction of the sediment particles in a time invariant coordinate system;

$U^s_{i,c}$ sediment velocity given in a time-invariant coordinate frame

U^s_c velocity of consolidating/swelling sediment particles (m/s)

$\tilde{U}^s_i$ apparent velocity of sediment particles in a time-varying coordinate frame (m/s)

$\tilde{U}^w$ apparent water velocity in a depth-adapted coordinate system (m/s)

ν^s_i diffusion coefficient for solid tracers (m^2/s)

ν^d_i diffusion coefficient for the dissolved tracer (m^2/s)

Q^s_i resuspension / deposition flux of the i-th fraction of particulate tracer [kg/(m^2 s)];

$\varepsilon_{i,w/b}$ void ratio of either fresh deposits or eroded bed

$\varepsilon_{i,bed}$ void ratio of the top sediment layer

$\varepsilon_{i,wc}$ void ratio of fresh deposits

z_{top} surface level of water column

z_{bot} bottom level of sediment bed

z_{bed} "sediment – water" interface

z_a bottom of an active sediment layer

h_a thickness of an active sediment layer

ε_m ultimate maximal void ratio of a self-weight consolidating sediments

T_c time scale of the sediment bed swelling/consolidation

$C_r^{\ s}$ actual sediment concentration at the reference level

$C_{eq}^{\ s}$ equilibrium reference concentration.

S_i' normalised excess skin friction

$\tau_{bi}^{\ \prime}$ skin friction (N/ m^2)

τ_{ci} critical shear stress for initiation of a non-cohesive sediment erosion (N/ m^2)

a empirical constant a = 0.002

d mean sediment diameter (m)

M resuspension rate on cohesive bed

τ_{ce} critical shear stresses of cohesive sediment erosion (N/ m^2)

τ_{cd} critical shear stresses of cohesive sediment deposition (N/ m^2)

u_{*c} friction velocity (m/s)

u_r reference velocity (m/s)

$z_o = \frac{k_N}{30}$ bottom roughness (m)

k_N Nikuradze roughness length (m)

η ripples height

λ ripples length

$C_{i,wc}^{\ s}$ sediment concentration in the near bottom water cell

$C_{i,bed}^{\ s}$ sediment concentration in an active sediment layer

α rate constant for mixing of the solid particled across "sediment – water" interface

β rate constant for mixing of the dissolved tracers across "sediment – water" interface

$\nu_o^{\ d}$ diffusion coefficient for mixing of the dissolved tracers across "sediment – water" interface

$\nu_o^{\ s}$ diffusion coefficient for mixing of the solid particles across "sediment – water" interface

ΔZ_{wc} thickness of the near bottom grid cell

ΔZ_{bed} thickness of the top sediment layer

Δ minimal thickness of sediment layer

$\hat{z}$ k-grid coordinates

$\tilde{z}$ sigma grid coordinates

p weighting constant

χ Van Karman constant 0.42

K diffusion coefficient ???

u_* shear velocity (m/s)

δ_w length scale of a turbulent wave bottom boundary layer (m)

Appendix H: Model parameters

Parameter	Description	Dimension	Cited values	Model values
ρ^w	Water density	[kg/(m^3 water)]	1025	1025
ρ_i^s	Sediment density	[kg/(m^3 solid)]	-	2650
ν_i^s	Vertical diffusion coefficient for solid particles in sediment bed	(m^2/s)	10^{-11} – 10^{-9}	10^{-10}
ν_i^d	Vertical diffusion coefficient for the dissolved tracers in sediment bed	(m^2/s)	10^{-11} – 10^{-9}	10^{-10}
W_{gi}	Settling velocity of suspended sediment particles (m/s)	m/s	10^{-1} – 10^{-6}	Sand: 0.2 – 0.003 Silt: 3 10^{-3} – 10^{-5}
A	Empirical constant in the formula for equilibrium concentration of non-cohesive sediments	nondim	10^{-5} – 2 10^{-3}	2 10^{-3}
Z_ref	Reference height in the formula for equilibrium concentration of non-cohesive sediments	m	3 ~ 7 (grain diameters)	7 (grain diameters)
M	Empirical constant in the formula for cohesive sediment resuspension	[kg/ (m^2 s)]	1.7 10^{-5} - 4.4 10^{-3}	$M = 0.002\tau_{ce}$
τ_{ce}	Critical shear stresses of cohesive sediment erosion	N/ m^2	0.05 – 5	0.2
τ_{cd}	Critical shear stresses of cohesive sediment deposition	N/ m^2	0.2 - inf	inf
z_o	Bottom grain roughness parameter	m	2 10^{-3} – 10^{-5}	(grain diameter) / 30
h_a	Thickness of an active sediment layer	m	0 – 0.007 (m), 0.5η	Max(0.005, 0.5η)
η	Ripples height	m	0 – 1	-
λ	Ripples length	m	0 – 10	-
$\varepsilon_{i,wc}$	Void ratio of fresh deposits	nondim	0.6 – 0.9	-
ε_m	Ultimate maximal void ratio of a self-weight consolidating sediments	nondim	0.4 - 0.6	-
T_c	Time scale of the sediment bed swelling/consolidation	day	-	1 – 100
ν_o^d	Diffusion coefficient for mixing of the dissolved tracers across "sediment – water" interface	m^2/s	-	ν_i^d
ν_o^s	Diffusion coefficient for mixing of the solid particles across "sediment – water" interface	m^2/s	-	ν_i^s
p	K-sigma grid weighting constant	Nondim	-	10^{-3} – 10^{-4}
χ	Van Karman constant	Nondim	0.42	0.42